Memoirs of the School of Engineering, Nagoya University
Vol.47, No.2 (1995)

INDUCTIVELY COUPLED PLASMA AS ATOMIZATION, EXCITATION AND IONIZATION SOURCES IN ANALYTICAL ATOMIC SPECTROMETRY

Hiroshi KAWAGUCHI

Department of Materials Science and Engineering

(Received October 30, 1995)

Abstract

Studies on inductively coupled plasma (ICP) for atomic emission and mass spectrometry accomplished in our laboratory since 1978 are reviewed. In emission spectrometry, the characteristics of the plasma are studied concerning the spatial profiles of spectral line intensity, axial profiles of gas and excitation temperatures, spectral line widths and matrix effect. The studies are particularly emphasized on the instrumentation such as developments of plasma generator, emission spectrometers, water-cooled torches and sample introduction methods. A slew-scan type spectrometer developed in these works represents a predecessor of the current commercial spectrometers. An ICP mass spectrometer was first developed in Japan in this laboratory in 1984. Non-spectroscopic interference of this method was found to have the correlation with the atomic weight of the matrix element. Plasma gases other than argon such as nitrogen and oxygen were used for the ICP to evaluate their performance in mass spectrometry as for the sensitivity and interferences.

Keywords: inductively coupled plasma, ICP-AES, ICP-MS, emission spectrometers, sample introduction, laser ablation, water-cooled torch

Contents

1. Introduction

The inductively coupled plasma (ICP) was first developed as an excitation source for emission spectrometry by Greenfield, et al.[1] and Wendt and Fassel[2] in 1964 and 1965, respectively. In those days, atomic absorption spectrometry (AAS) developed by Walsh in 1955 was gaining increasing popularity as a sensitive elemental analysis method of solutions. On the other hand, classical atomic emission spectrometry (AES) using light sources such as arc and spark was loosing interest in the analytical community because of the poor precision and the difficulties in the solution analysis. A new approach, ICP-AES, therefore, did not attract a much attention at the beginning.

In 1969, Dickinson and Fassel[3] reported the emission spectrometric detection of the elements at the nanogram per ml level using the ICP excitation. They described a toroidal shaped plasma of the ICP in which a doughnut-hole was punched in the center of the plasma by a central gas flow. Aerosols of sample solutions are effectively introduced into this hole and this gives the most important origin of various excellent analytical performance of ICP. The paper became one of the landmarks in the development of ICP-AES, and since then, a large number of researchers in the world began their studies on the fundamental characteristics and application to the practical analysis. The situation of ICP-AES in those years is often called as "the Renaissance" of an old approach, atomic emission spectrometry.

In 1980, atomic mass spectrometry (MS) of solutions was proposed by the group of Fassel[4] using the ICP as an ion source. In early 1970s, there were already ample documents describing the high temperature (*ca.* 6000 K) of the ICP, in which analyte elements were highly ionized. If the ions in the plasma are efficiently introduced into the vacuum chamber, a sensitive analysis by MS will be performed for the elements in solutions. The efficient sampling of ions from the high-temperature plasma was difficult at first since the sampling orifice (50 μm i.d.) was easily clogged with the salt in the sample solutions. The difficulties have been overcome by employing a larger orifice and 3-stage differential evacuation system[5], which are the common practice in the present commercial instruments.

In 1975, we started to construct an ICP generator for AES by ourselves, which we believe was the first attempt in Japan. There was no ICP instrument including imported ones in those days. Since then, our research have extended from the fundamental studies of the ICP to the development of an ICP mass spectrometer in 1983. This paper will describe an overview of our achievements on ICP-AES and ICP-MS during last 20 years.

2. Generation of Inductively Coupled Plasma

2. 1 Principle

Although many books[6–8] and reviews[9,10] have been published on the ICP, the principle of the ICP generation will be briefly described here for convenience to readers who are not familiar in this field. The plasmas are defined as gases in which a significant fraction of their atoms or molecules is ionized and the charge of the positive ions and electrons are balanced so that the plasmas are neutral as a whole. Therefore, the plasmas are electrically conductive and interact with high-frequency magnetic fields, analogous to the inductive heating of a metal cylinder.

In order to form an ICP, a quartz tube approximately 2 cm in diameter is placed inside a coil connected to a high-frequency generator operating at 5—40 MHz and output power of 1—4 kW. When the generator power is turned on after flowing Ar inside the tube, nothing happens because Ar is a nonconductor. A seed of electrons is necessary to be planted in the coil space by tickling the tube with a Tesla coil. If the proper flow pattern of Ar is maintained inside the tube, the plasma is formed spontaneously at the open end of the tube.

The high-frequency current flowing in the induction coil generates a oscillating magnetic field whose lines of force are axially oriented inside the tube. The induced magnetic fields, in turn, induce the currents (eddy currents) to flow in closed annular paths inside the plasma and ohmic heating of the gas occurs. The plasma formed in this way attains a gas temperature of *ca.* 10000 K in the region of maximum eddy current flow.

To prevent overheating of the quartz tube by the plasma and to introduce sample aerosols into it, an assembly of concentric quartz tubes, called as "torch", is used as shown in Fig. 1. The argon flows consist of the outer gas, intermediate gas and carrier gas. The outer gas flow of 10—15 l/min serves to cool the inside wall of the outer tube and to center the plasma radially in the tube. The intermediate gas flow is typically 1 l/min and some times

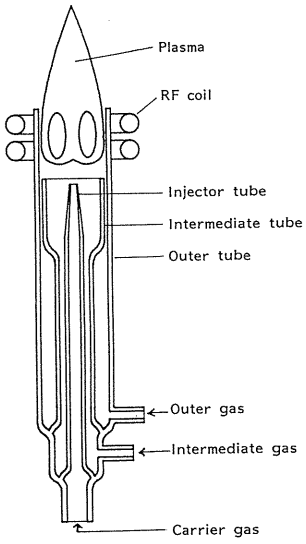

Fig. 1. Schematic diagram of ICP torch and plasma.

omitted. It has an auxiliary role to float the plasma slightly from the intermediate tube. The central flow, carrier gas, is used to transport the sample aerosols to the plasma and the flow rate is also about 1 l/min.

If the plasmas are to be used as excitation sources for emission spectrometry, samples should be efficiently injected into the plasma and should remain in the interior of high temperature region as long as possible. This condition is usually difficult to attain because the cold sample aerosols tend to pass around the surface of the plasma due to a combination of magnetic and thrust pressure, and viscosity effect.

With the torch as shown in Fig. 1 and proper tip shape of the central tube, a hole is punched through the center of the plasma by a central gas flow. The skin-depth effect of induction heating is considered to be important for the development of the hole. The eddy current tends to flow more closely to the outer portion of the plasma, which is shown by the equation,

$$J = J_0 \exp(-x/\delta) \tag{1}$$

where J_0 is the current density at the surface of the conductor, x is the distance from the surface and δ is the skin depth. The eddy current declines to 1/e of its maximum value near at the skin depth,

$$\delta = 1/(\pi f \mu \sigma)^{1/2} \tag{2}$$

where f is the current frequency, μ is the permeability and σ is the conductivity. As shown in Equ. 2, the skin depth is reciprocally proportional to the square root of the current frequency. For the 10000 K argon plasma, the depth is calculated to be *ca.* 2 mm at the frequency of 27 MHz.

Since the hole possesses a lower temperature than the doughnut body, it offers less resistance to the injection of sample aerosols. Thus the samples are quite efficiently injected into the ICP. As the sample aerosols travel upstream through a narrow axial channel, analytes are led to a complete vaporization and a high degree of atomization and ionization.

2. 2 High-Frequency Generator and Matching Circuit

Although the most of the commercial high-frequency generators currently used for ICP are constructed with solid state components, we designed a generator circuit with vacuum tubes in 1975.[11] The block diagram of the generator circuit is shown in Fig. 2, which consists of a crystal oscillator, a buffer amplifier and a power amplifier.

A high-frequency voltage of 27.12 MHz is generated by the crystal oscillator using a miniature vacuum tube, 5763, and amplified by a buffer amplifier using a power tube, 2B46. The final power amplifier using a vacuum tube, 7F37R (Toshiba, max. plate loss of 1 kW) works at C-class and generates a maximum power of 1.5 kW. In order to stabilize the output power, a feedback circuit is incorporated to control the screen grid voltage of the 7F37R tube. The output power and reflected power are monitored by a transmission-type power meter. The output impedance of the generator is adjusted to 50 Ω to send the high-frequency power to a matching circuit through a coaxial cable of the same impedance.

A high-voltage supply for the final power tube consists of a three-phase bridge rectifier and generates a dc voltage of 4.5 kV and maximum current of 1 A. When this high voltage was used without a ripple filter, a loud audible sound was generated from the plasma torch. The ripple voltage, therefore, had to be reduced to less than 2 %.

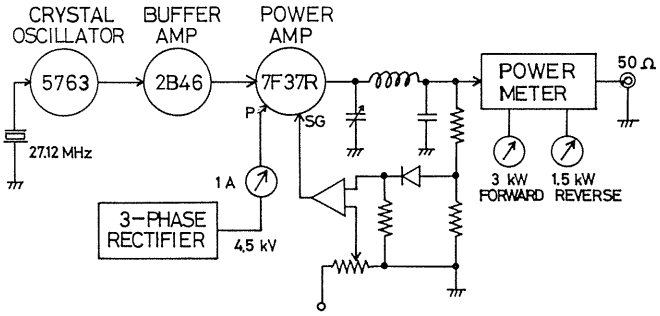

Fig. 2. Block diagram of high frequency generator for ICP.

Since the impedance of the fully developed plasma is around 1 Ω, a matching circuit is necessary to transform the output impedance of the generator, 50 Ω, into that low value. Moreover, the work coil impedance is quite high before the plasma is ignited and rapid tuning of the matching circuit is necessary after the plasma is ignited. A matching circuit we constructed is shown in Fig. 3. The 3-turn input coil and 2-turn work coil were prepared from 6-mm o.d. copper tube to allow the water cooling. A precise adjustment of the tap position at the input coil was necessary in the beginning to ignite the plasma. After the plasma was ignited, a large impedance change in the work coil was compensated by tuning the air capacitor and monitoring the reflected power. The reflected power could be reduced less than 10 W when the output power was 1.2 kW. A commercial matching circuit currently used consists of an input shunt air-capacitor and a series vacuum-capacitor. Once the air capacitor is tuned properly, only the vacuum capacitor is necessary to be tuned when the plasma is ignited. In a state-of-the-art matching box, the vacuum capacitor is automatically tuned by a servomotor so as to reduce the reflected power to minimum.

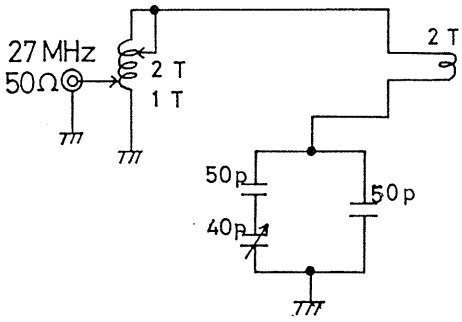

Fig. 3. Matching circuit constructed.

With the ICP source described above, analytical characteristics of ICP-AES for phosphorus were studied.[11] In spite of the primitive equipments, a dynamic range of the calibration curve for phosphorus obtained was more than 4 orders of magnitude and the detection

limit was 0.12 μg/ml. Phosphorus contents in various samples such as starch, coffee powder, and milk were determined and their values were excellently agreed with the values determined by spectrophotometric method.

The relative standard deviation of spectral intensities was around 1 %, which was excellent considering that a home-made equipment and a demountable torch were used. The RF generator, however, was not so stable as the current commercial one which employing a negative feedback circuit extensively. The C-class amplifier we used seemed not to be satisfactorily stabilized for ICP-AES.

3. Characteristics as Emission Source

3. 1 Temperature

3. 1. 1 Method for the Temperature Measurement

Temperature is one of the most important characteristics of high temperature plasmas and it has also been studied for the ICP by many authors. Since the ICP has its unique configuration as described in Section 2.1, it should also have a unique spatial distribution of the temperature. Apparently, axial profile of the temperature has the most significant effect on the emission signals of analytes because analytes are introduced into the axial channel of the plasma.

There are several methods for the measurement of the temperature of plasmas[12] including spectroscopic method. Spectral line intensity can be expressed as

$$I = N_n A_{nm} h\nu \tag{3}$$

where N_n is the population of atoms in the excited state, n, A_{nm} is the transition probability from the n to the m state for spontaneous emission, h is the Planck's constant and ν is the frequency of the spectral line. If the local thermal equilibrium (LTE) is assumed in the plasma, N_n can be written by Boltzmann equation,

$$N_n = N g_n \exp(-E_n/kT)/ Z \tag{4}$$

where N is the total population of atoms, g_n is the statistical weight of the n state, E_n is the excitation energy, k is the Boltzmann's constant, T is the plasma temperature and Z is the partition function. Combining (3) and (4), we obtain,

$$I = N g_n A_{nm} h\nu \exp(-E_n/kT)/ Z \tag{5}$$

When the intensities of many spectral lines of an element (thermometric species) introduced into a plasma are measured and the values of $\log(I/g_n A_{nm}\nu)$ are plotted against the E_n (called as the Boltzmann plot), a straight line will be obtained and the plasma temperature T can be calculated from the slope of the line. More conveniently, T can be calculated from the measurement of the intensity ratio of two lines which have different excitation energies. The lines employed in this experiments[13] are Fe I 381.58, Fe I 382.44, OH 307.70 and OH 307.30 nm, where iron lines are used to measure the excitation temperature and OH molecular lines are used for the gas temperature. If the LTE prevails in the plasma, the two temperatures will coincide with each other.

3. 1. 2 Instrumentation and Procedure

Axial channel of the ICP was imaged onto the entrance slit of a 1-m grating monochromator by a quartz lens with a demagnification of 0.26. The observation height was scanned by slicing the image of the plasma with a vertically movable horizontal slit (0.3-mm opening) placed in front of the entrance slit. The schematic diagram of the movable slit and driving mechanism is shown in Fig. 4.[13] The horizontal slit was driven over a distance of 9.1 mm from bottom to top by a stepping motor controlled by a computer. The emission signal intensities were measured at every step of the 0.15 mm movement of the slit, and the data were acquired by a computer to be processed. A solution containing 1 mg/ml Fe as a thermometric species was nebulized and introduced into the plasma. The OH molecular lines are always observed because water is also introduced into the plasma.

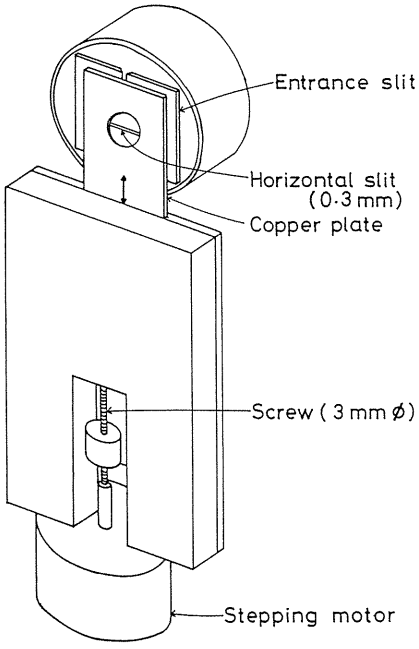

Fig. 4. Schematic diagram of moving slit and driving mechanism for the measurement of axial emission profiles.

3. 1. 3 Axial Profiles of Emission and Temperature

The axial emission profiles of Fe I 382.4 nm and OH 307.3 nm lines are shown in Fig. 5a as a function of the height above the load coil and the excitation and gas temperatures calculated from these profiles are shown in Fig. 5b.[13] The excitation temperature profile has a peak at about 15 mm above the load coil and the gas temperature has no apparent peak but gradually increases with the height. The gas temperature is considerably lower than the excitation temperature which indicates that no LTE prevails in the argon ICP.

In Fig. 6, axial emission profiles of two Fe I lines as well as excitation temperature profiles calculated from these lines are shown for three different levels of RF power. Note

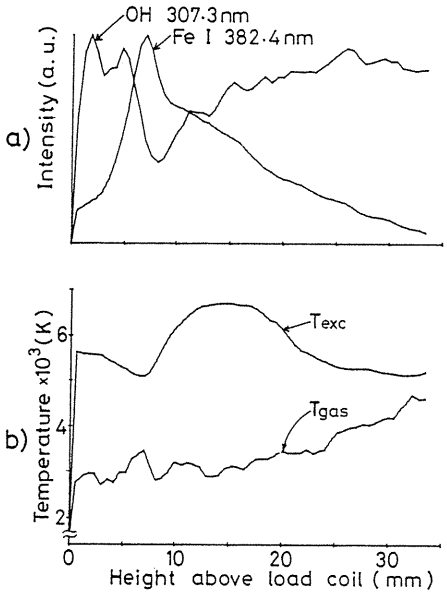

Fig. 5. Axial emission profile of a) Fe I and OH lines, and b) calculated excitation (T_{exc}) and gas (T_{gas}) temperatures.

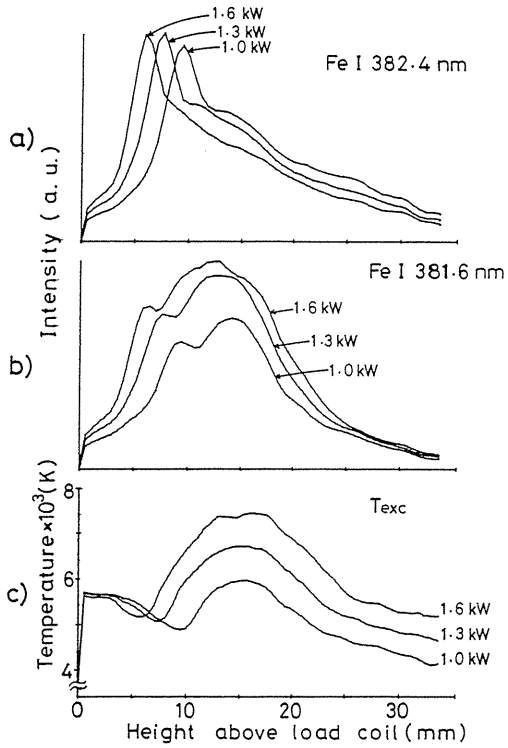

Fig. 6. Axial emission profiles of a) Fe I 382.4 nm, b) Fe I 381.6 nm lines and c) temperature for the RF power of 1, 1.3 and 1.6 kW.

that the two iron lines exhibit different axial profiles because of the different excitation energies. The Fe I 382.4 nm line has a lower excitation energy (3.24 eV) than that of the Fe I 381.6 nm line (4.73 eV). The line of the lower excitation energy shows the emission peak at the lower position in the plasma than the line of the higher excitation energy. With increasing RF power, the position of the emission peak goes down further and this is more clearly seen for the lower excitation energy line.

The excitation temperature has a peak at about 15 mm above the load coil, which means that the axial channel of the ICP is not heated enough at the load coil region where the RF energy is supplied. Many researchers have shown that the radial temperature profile near the load coil has a dip at the center. The peak temperature is about 6000 K at RF power of 1 kW and increases with the power. Interestingly, the peak position from the load coil is little affected by the power.

The excitation temperature profiles are also affected with the operating conditions of the ICP other than the power. Especially, the most important effect is the carrier gas flow rate, which is shown in Fig. 7.[13] The emission profiles of Fe lines are greatly affected with the carrier gas flow rate and the effect is different for each of these lines with different excitation energies. Correspondingly, the temperature changes significantly, usually decreases, as the

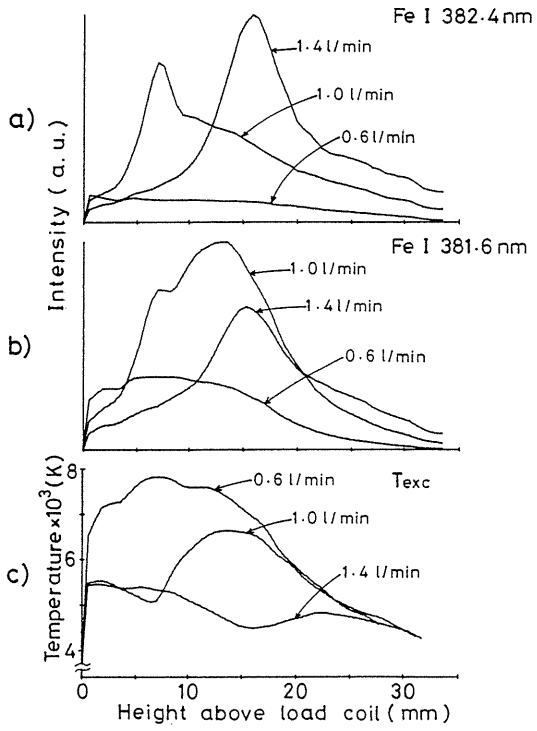

Fig. 7. Effect of the carrier gas flow rate on axial profiles of Fe I lines and excitation temperature.

flow rate increases and the position of the temperature peak shifts upward. The effect of the carrier gas flow rate is so significant on the temperature and then on the emission intensity that the flow rate must be critically controlled to keep it constant, usually, at 1.0 l/min.

3. 2 Spectral Line Width

3. 2. 1 Method and Instrumentation

Spectral interference in ICP-AES is often a serious problem when it is applied to samples of complex composition. The problem may be reduced by using a spectrometer with high resolving power and dispersion provided that the spectral lines emitted from the ICP are sufficiently narrow. Since the temperature of ICP is more than 6000 K as shown in the previous section, the lines will be suffered from Doppler broadening and the effect of the Stark broadening must also be considered because there is a high electric field in the plasma.

To measure the line profile, a pressure-scanning Fabry-Perot interferometer (Mizojiri Kogaku) crossed with a monochromator (0.5-m Ebert mounting) was used.[14] The interferometer was consisted of a pressure chamber with quartz windows and a pair of parallel quartz plates (60 mm dia., nominally flat to $\lambda/100$). The plates were coated with aluminum and a protective layer of magnesium fluoride. The transmittance of the plates were 0.7 % at 600 nm, 1.5 % at 400 nm, 3.1 % at 300 nm and 7.6 % at 200 nm. Quartz spacers of 3.020 mm were used for the wavelengths below 300 nm and of 6.055 mm for other lines.

Light from the ICP was collimated by a spherical quartz lens and led to the interferometer. Interference fringes were focused onto the entrance slit of the monochromator. The slit of the monochromator was opened widely and a thin plate with a pin-hole of 0.4 mm in diameter was placed on the entrance slit. The interferometer was scanned by introducing air into the pressure chamber through a needle valve after the chamber was roughly evacuated by a rotary vacuum pump.

The full width at half maximum (FWHM) of a spectral line was measured with a scale from the interferogram and converted into wavelength by referring the free spectral range ($\Delta\lambda_{free} = \lambda^2 / 2nt$, where refractive index $n = 1$ for air and t is the spacer length).

In order to estimate the instrumental broadening, we assumed that the line widths emitted by hollow-cathode lamps operated at 6 mA were purely Doppler broadened at 400 K and calculated by

$$\Delta\lambda_D = (2\lambda / c)(2RT \ln 2 / M)^{1/2} \tag{6}$$

where c is the light velocity, R the gas constant, T the temperature, 400 K and M the atomic weight.

It has been shown that instrumental broadening is predominantly Lorentzian and that the experimental profiles give a Voigt profile. Since the profile of a line with the Doppler broadening is Gaussian, the instrumental FWHM can be calculated from the relation of the FWHM of Voigt profile with those of Lorentzian and Gaussian.

$$\Delta\lambda_{ins} = (\Delta\lambda_{exp}{}^2 - \Delta\lambda_D{}^2 / \ln 2)^{1/2} \tag{7}$$

where $\Delta\lambda_{ins}$ is the instrumental width, $\Delta\lambda_{exp}$ the experimental width and $\Delta\lambda_D$ the Doppler width calculated by Equ. 6. Once the instrumental width is obtained by the measurements of a line profile from a hollow-cathode lamp, the actual width of a line emitted from ICP can be calculated by

$$\Delta\lambda_{act} = \{\ln 2(\Delta\lambda_{exp}{}^2 - \Delta\lambda_{ins}{}^2)\}^{1/2} \tag{8}$$

3. 2. 2 Widths of Lines from Hollow-Cathode Lamps and ICP

As an example, profiles of the Cd 228.80 nm line from a hollow-cathode lamp are shown in Fig. 8.[14] Self-reversal is clearly observed for a lamp current of 8 mA or more but the FWHM does not appreciably change for a current of less than 6 mA.

By introducing solutions of various elements into the ICP, the FWHMs of the lines of these elements were measured. The actual halfwidths of the lines emitted from the ICP, which are corrected with instrumental width, are plotted against the Doppler width at 5000 K of these elements as shown in Fig. 9.[14] The dashed lines in Fig. 9 indicate the relation between the FWHM of the Voigt and Gaussian profiles as a function of the "a"-parameter. The line widths measured in this experiment were reasonably agreed with the literature values that were already reported and, later, they were confirmed by researchers who measured the line widths with the other principle.

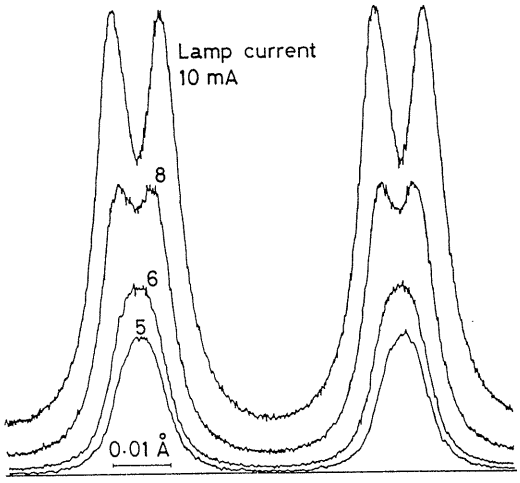

Fig. 8. Line profiles of the Cd I 228.80 nm line emitted by a hollow-cathode lamp operated at various currents. Spacer of etalon: 6.055 mm.

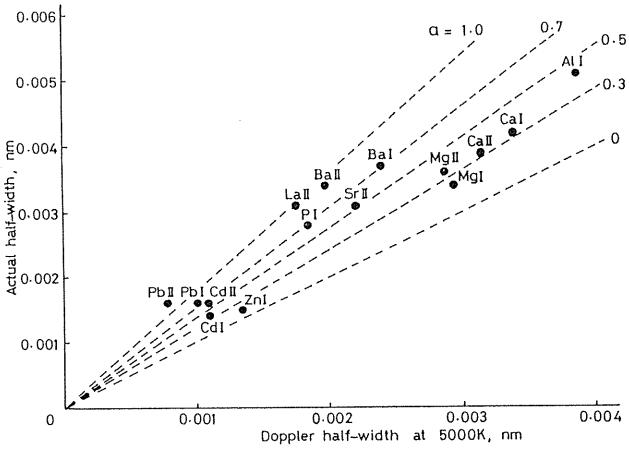

Fig. 9. Relationship between the actual FWHM for lines emitted by ICP and the Doppler width for 5000 K.

3. 3 Non-Spectroscopic Matrix Effect

3. 3. 1 Effect of Easily Ionizable Elements

From the early stage of its development, ICP was found to suffer at minimum extent from chemical interference effect, such as the effect of calcium on the phosphorus determination. It was explained by the fact that sample aerosols were completely vaporized during their passage through a central channel of the plasma. Some researchers, however, reported the effect of potassium on analytes of other elements in ICP-AES and both the enhancement and

suppression effects were found depending on the operating conditions. Easily ionizable elements such as lithium, potassium and sodium, which have relatively low ionization potentials, have been known to cause the ionization interference effect also in the classical emission spectrometry with arc or spark excitation.

In order to clarify the mechanism of the interference, axial profiles of the emission from the ICP were observed with and without matrix elements.[15] The axial profiles of the emission were measured with a monochromator attached with a photodiode array detector at the exit slit. Since the instrument will be described in Section 4.3 in more detail, only the experimental conditions are briefly described here. The axial part of the ICP was imaged onto the entrance slit of the monochromator (0.25-m grating) by quartz lenses with a demagnification of 1/5. A 512-element self-scanning linear photodiode array was mounted vertically at the focal plane of the monochromator replacing the exit slit. Signals are integrated by the array for 1–3 s and acquired by a small computer.

Spatial profiles of Ca I 422.7 nm and Ca II 393.4 nm lines are shown in Fig. 10 at various lithium concentrations.[15] With the increase of lithium concentration, the emission intensity of the neutral atom line, 422.7 nm, increases significantly near the peak of the profile, but only a slight effect in the region of 15–20 mm above the load coil. The emission intensity of the ion line, 393.4 nm, on the other hand, shows the enhancement effect until 18 mm from the load coil, while it shows the suppression effect above 18 mm.

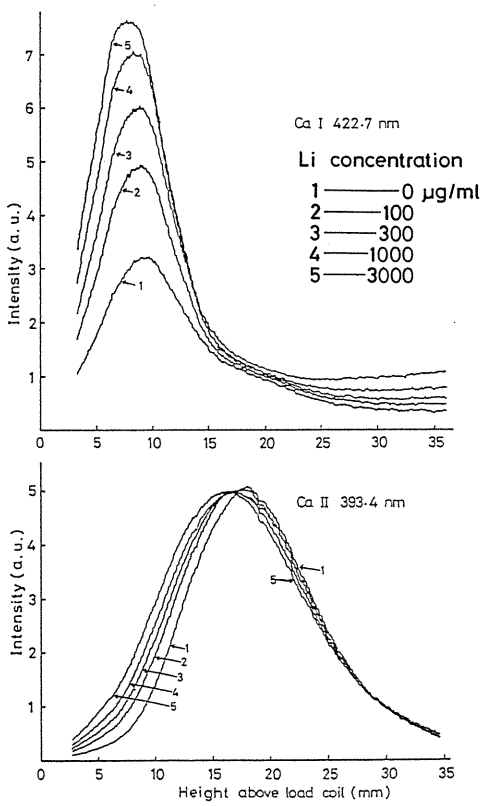

Fig. 10. Spatial profiles of calcium emission as a function of lithium concentration.

These experimental results explain why the enhancement or suppression effect is observed depending on the operating conditions. If the proper observation height is selected for ion lines, no interference effect of easily ionizable elements will be found by compensating the enhancement and suppression effect to each other. The crossing point from enhancement to suppression was found to move with the excitation energy of lines, carrier gas flow rate or RF power. Though the effects of the easily ionizable elements in ICP-AES have then been extensively studied by many researchers, the mechanism of the interference effect still remains unclear.

3. 3. 2 Effect of Sulfuric Acid

Acid concentration of sample solution has sometimes shown an interference effect in ICP-AES. Since the largest effect was observed from sulfuric acid among the inorganic acids, spatial profiles of calcium emission were measured as a function of its concentration. The results shown in Fig. 11 indicate that the sulfuric acid depresses the emission over the whole observation height at the same extent both for the neutral and ion lines.[15] This means that the depression is caused by the decrease in the analyte concentration in the plasma. Comparing Fig. 11 with Fig. 10 the difference in the interference mechanisms in both cases is apparent.

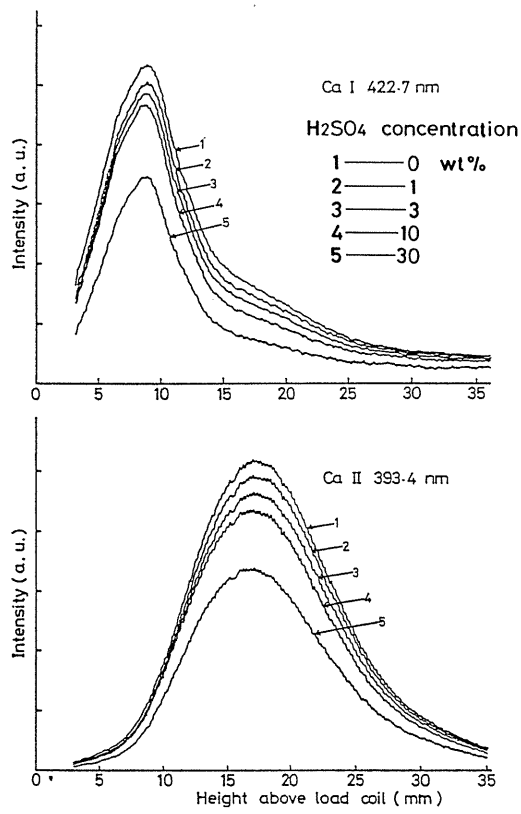

Fig. 11. Spatial profiles of calcium emission as a function of sulfuric acid concentration.

The decrease in the analyte concentration with increasing sulfuric acid may be caused by the nebulization interference effect. The characteristics of the sample solution such as viscosity and surface tension are known to affect the distribution of the diameter of liquid aerosol and, therefore, the nebulization efficiency. As the increase of the sulfuric acid concentration, viscosity of the sample solution increases and this causes the decrease in nebulization efficiency.

3. 4 Effect of Organic Solvent

3. 4. 1 Variation of Plasma Impedance

When an organic solvent is introduced into the ICP, the plasma often becomes unstable and is sometimes extinguished when the operating conditions are not properly chosen. To make the reason clear, the variation of the plasma impedance with the increase of the organic solvent loading was investigated.[16)]

An equivalent circuit of a conventional matching unit of the ICP generator is shown in Fig. 12, where L_w is the load coil inductance, L' and R' the stray inductance and resistance of lead wire, and L_p and R_p the inductance and resistance of the plasma, respectively. The input impedance of the matching circuit during the plasma ignition can be expressed as,

$$Z = \frac{RA + DB}{A^2 + D^2} + j\frac{AB - RD}{A^2 + D^2} \tag{9}$$

where,

$$A = (C_1 + C_2)/C_1 - \omega^2 L C_2 \tag{10}$$

$$B = \omega L - 1/\omega C_1 \tag{11}$$

$$D = R\omega C_2 \tag{12}$$

$$R = R' + SR_p \tag{13}$$

$$L = L_w + L' - SL_p \tag{14}$$

$$S = \omega^2 M^2/(R_p{}^2 + \omega^2 L_p{}^2) \tag{15}$$

and M is the mutual inductance between load coil and plasma, and ω the angular frequency of the power.

By measuring the values of C_1 and C_2 when the matching circuit is tuned for zero reflecting power, the value of R, the reflected resistance or the resistance of the plasma observed from the input terminal of the matching circuit, can be determined so as the input impedance, Z, to become $Z = (50 + 0j)\ \Omega$. This calculation was repeated iteratively by a computer, by successively increasing the value of R from 0 until the error becomes less than 0.1 %.

The reflected resistance, R, was measured for the aqueous solutions of various ethanol concentrations at several RF power. Since the value R decreases with the increase of R_p as is expected from Equ. 13, the results indicate that the plasma resistance increases with the increasing ethanol concentration. The effect of the ethanol on the plasma resistance becomes less significant as the power increases. These results agreed well to the experimental observation in the plasma operation.

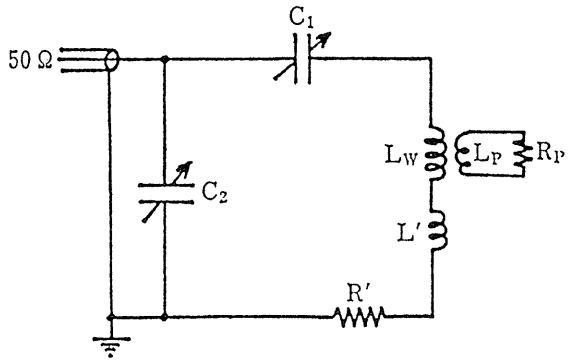

Fig. 12. Equivalent circuit of matching unit.

Difficulty in tuning the matching network, encountered when organic solvents are introduced into the ICP, can be explained by the change in the slope of the tuning curve. This is also caused by the change in the plasma impedance. When the proposed tuning procedure was adopted, the difficulty was considerably avoided.

3. 4. 2 Spectral Interference

Spectral interferences from molecular band systems are not generally significant in ICP-AES when aqueous sample solutions are introduced. When organic solvents are introduced, however, molecular bands such as CN, C_2 and NH appear in the wavelength region higher than 330 nm. Rare earth elements and yttrium have their strong lines in this wavelength region, so that these molecular bands often interfere with the measurements of these elements.

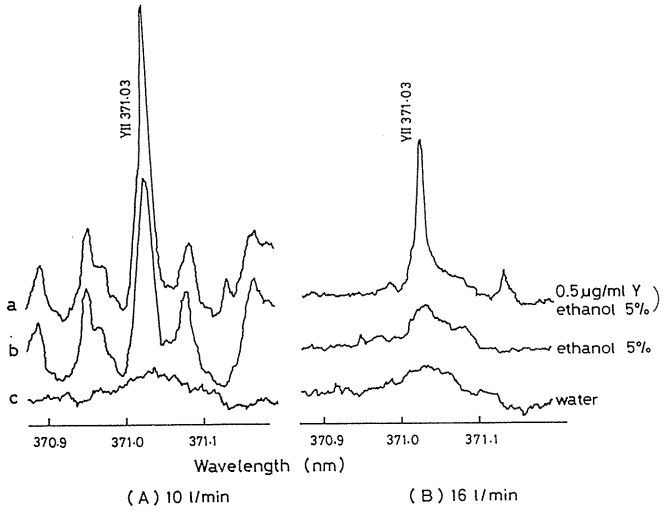

Fig. 13. Wavelength scans around the Y II 371.03 nm line. Solutions: a: 0.05 μg Y/ml in 5 % ethanol, b: 5 % ethanol, c: water. Outer gas flow rate: (A) 10 l/min, (B) 16 l/min.

Wavelength scans around the Y II 371.03 nm line are shown in Fig. 13[17] recorded with a high-resolution echelle grating monochromator. The characteristics of the monochromator will be described in Section 4.2. At the relatively lower outer gas flow rate, 10 l/min, molecular band, CN, appears when 5 % ethanol solution is introduced. The CN band emission severely interfere with the yttrium line. The CN molecules may be generated by entrainment of nitrogen in air into the plasma and reacting with carbon originated from decomposed ethanol. If the plasma is shielded by the higher flow rate of outer gas, 16 l/min, the CN band strongly suppressed as shown in Fig. 13B.

The CN band emission at the 388.34 nm band head increases with the increase in the concentration of organic substances in water. At the same concentration of organic substances, the CN band emission increases with the order of citric acid, acetic acid, methanol, ethanol and acetone. This order is determined by the vapor pressure of the substance and carbon content in the sample.

4. Emission Spectrometer

4. 1 Development of Slew-Scan Spectrometer

4. 1. 1 Concept of the Spectrometer

Simultaneous multielement analysis is one of the distinctive features in AES and photographic emulsion was classically employed as detector in this method. Although multichannel spectrometer with photomultipliers as detector was developed in 1950s, it is not convenient in research laboratories because of the limited number of channels and the lack of flexibility. The polychromators usually have 20—40 fixed exit slits and detectors corresponding to the wavelengths of the spectral lines of elements to be determined. The exit slits are installed at the factory of the manufacturer and difficult to be changed for other wavelengths in analytical laboratories. Since the number of the slits are limited not only by the space at the focal plan of the spectrometer but also by the economy, the flexibility in selecting analytical lines is quite limited. Therefore, the polychromators are mainly used in the laboratories for control analysis, but not in the research laboratories.

With a monochromator, however, sequential analysis of many elements is not so easy, because it is time consuming and needs some experience to adjust exactly the wavelength of the monochromator. As the availability of small computers is gradually increased, laboratory automation has come to be realized in some institutions in early 1970s. It was just the same time that ICP-AES was rapidly growing for a new generation. Since the ICP produces steady signals with time, a multielement analysis can be performed in a sequential mode if the wavelength of the monochromator can be rapidly changed from one element to another. The developing concept of a computer-controlled monochromator described above was realized in this study[18] by modifying a 0.5-m grating monochromator and using a minicomputer. Most of the current commercial sequential spectrometers for ICP-AES are based on the similar concept and usually called as slew-scan spectrometers.

4. 1. 2 Modification of Conventional Monochromator

A commercial grating monochromator (Nippon Jarrell-Ash, 0.5-m Ebert mounting) was employed for the construction of a computer-controlled programmable monochromator.[18] First of all, the wavelength driving motor of the monochromator was replaced by a stepping motor (Nippon Pulse Motor Co., PF6-36) which could be driven by the maximum rate of

1000 steps/s and 72 steps/revolution. The first and second reducing gears of the original monochromator were replaced by plastic ones to reduce the inertia and the gearshift mechanism was removed. Since the monochromator with a grating of 1200 grooves/mm has a reciprocal linear dispersion of 1.6 nm/mm, one step of the pulse motor resulted in a wavelength change of 0.00347 nm. Therefore, the wavelength can be changed at the maximum rate of 4.47 nm/s, which means the driving time from 200 to 400 nm is *ca.* 45 s.

Even though the wavelength change for one step of the pulse motor is small compared to the spectral band width (0.048 nm at a slit width of 30 μm), automatic adjustment of the wavelength exactly to a spectral line is not easy. In order to scan a narrow wavelength region, a quartz vibrating plate shown in Fig. 14[19] was mounted behind the entrance slit of the monochromator. The quartz plate, 2 mm thick, oscillates at a resonance frequency of *ca.* 97 Hz, when the magnetically induced voltage in the pickup coil is amplified and fed to the drive coil. With this plate, about 0.3 nm range of the wavelength at maximum can be repetitively scanned.

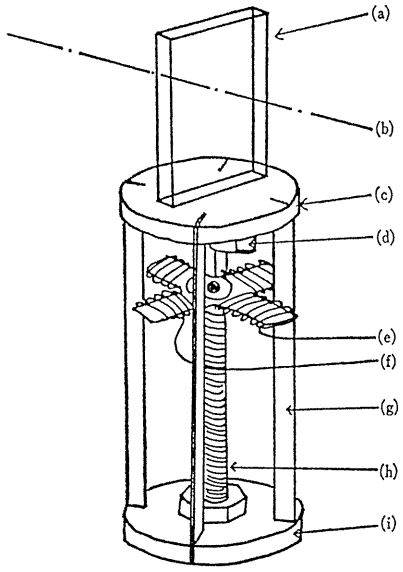

Fig. 14. Mechanical vibrating plate for optical scan. a: quartz plate, b: light path, c and i: brass, d: magnet, e: pickup coil, f: drive coil, g: phosphor bronze plate, h: stand off.

A block diagram of the whole system is shown in Fig. 15.[18] A minicomputer (HITAC 10 II) with 16-bit 8-k word memories was used to control the stepping motor via a driving unit, quartz vibrating plate, data acquisition and data processing. A control unit[20] was constructed to interface the output of D/A converters with the driving units of the stepping motor and the quartz plate, and a strip chart recorder.

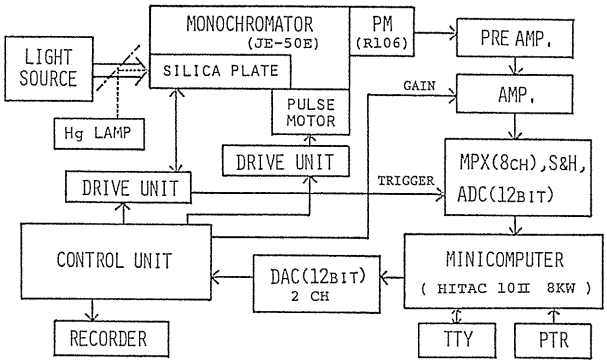

Fig. 15. Block diagram for computer-controlled programmable monochromator.

4. 1. 3 Software and Performance

A 6-figure wavelength table of the 3 strongest spectral lines for each of 71 elements was stored in the memory. Spectral lines of interest can be selected from the memory by typing the symbols of the element and the number designated to each of the 3 lines. Lines that are not in the memory can also be used by typing the wavelengths. Computer rearranges the retrieved list of the wavelength in ascending order and calculates the numbers of motor steps necessary to slew the monochromator from a reference line to the selected lines. All the program was written with an assembler language and divided into two parts, wavelength selection and data acquisition due to the lack of the memory capacity (8 k words).

Wavelength calibration of the monochromator was automatically performed with the Hg 253.652 nm line from a mercury lamp. The computer moves the wavelength to the first line and acquires the signal from the detector synchronizing with the vibration of the quartz plate. In each half cycle of the vibration, 91 data are acquired and stored in individual locations in the storage. Thus a spectral region, 0.1−0.3 nm, optically scanned by the quartz plate is digitized in 91 memories.[21] After the predetermined number of scans has been completed, the monochromator is scanned to the next line and the procedure is repeated.

Using a mercury hollow-cathode lamp as light source, spectral line profiles for 9 Hg and 2 Ne lines were measured with the results shown in Fig. 16.[18] A mercury doublet, Fig. 17E, shows the resolution of the spectrum when the slit width of the monochromator is 10 μm. Error in wavelength setting can be determined from the shift of the peak position from the center in each profile. The errors measured from several runs of operation were less than 0.02 nm. The largest origin of the error was considered to be the error of the precision screw of the monochromator, because the error curves against the wavelength have a reproducible pattern. The error due to the loose contact between the sine bar pivot arm and the nut on the precision screw causes the scatter of the error curves. These errors cannot be easily eliminated even by rigorous modification of the wavelength drive mechanism. Since the present system measures the profiles of spectral lines, the error in the wavelength setting does not cause the error in the measurement of the peak intensity.

The present system was applied to various analytical tasks, one of which was the determination of trace heavy metals in water after preconcentration.[22]

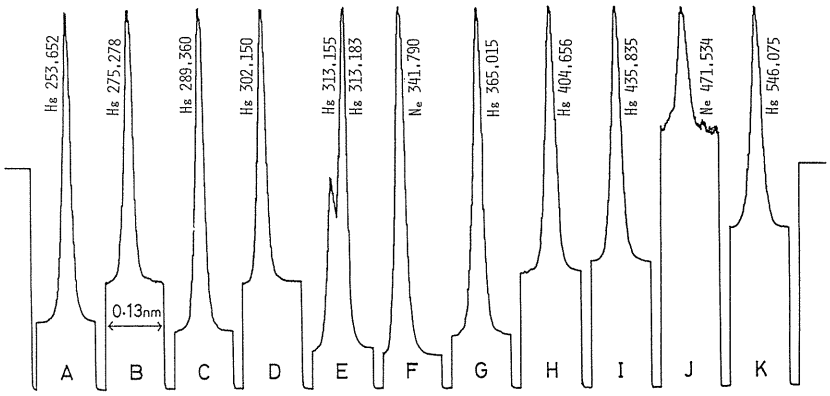

Fig. 16. Spectral profiles of various lines from a Hg hollow-cathode lamp.

4. 1. 4 Data Processing with Slew-Scan Spectrometer

Although a profile of the spectral line consisting of *ca.* 90 data can be measured with the present system, only a few data at the peak and background are needed for the measurement of the analytical line intensity if there is no interference line is observed. In order to utilize the data more efficiently and to decrease the measurement error, various curve fitting methods were tried to apply for the accurate measurements of the peak intensity.[23)]

The 9 data points around the peak of a line profile measured with the present system were fitted to parabolic, Lorentzian and Gaussian curves to calculate the exact peak values and to compare the relative standard deviation (RSD). In preliminary experiments, a weak mercury line, Hg 289.36 nm, is selected using a mercury lamp and the profiles are measured repeatedly. The RSDs of the peak values for original profiles and parabolic, Lorentzian and Gaussian fitting curves were, 6.6, 5.9, 3.9 and 3.8 %, respectively. Obviously, Gaussian fitting method was the best and this method was proposed. In this fitting calculation, a fixed halfwidth of the line determined from a profile of the Hg 253.6 nm line was used because the real widths of spectral lines was far less than the spectral band width of the monochromator.

4. 2 Characteristics of Echelle-Type Grating Spectrometer

4. 2. 1 Principle

Echelle-type grating spectrometer was first developed by Harrison in 1949 but commercial instruments have been available only after 1969 when SpectraMetrics Co., USA, developed an emission spectrometer with a dc plasma light source.[24)] When a grating is used in such a way that the incidence and diffraction angles are nearly equal, i.e., $\alpha = \beta$, the grating equation becomes to

$$m\lambda = 2d \sin \beta \tag{16}$$

where the m is the order and d is the grating constant. Therefore, the angular dispersion is obtained by,

$$d\beta/d\lambda = (\tan \beta)/\lambda \tag{17}$$

This equation shows that the angular dispersion becomes larger as the diffraction angle increases. Echelle grating is designed to be used with a large diffraction angle and at high order numbers.

In order to separate the different order spectra, an echelle grating spectrometer is usually constructed with cross dispersion by using a crossed prism or grating. In cross-dispersed spectra, a free spectral range can be calculated by,

$$\Delta\lambda_F = \lambda^2 / 2t \tag{18}$$

where, t is the groove depth of the echelle grating.

4. 2. 2 Optical Characteristics

A computer-controlled echelle-grating monochromator was first developed in Japan in 1980 by Kyoto Koken Co. The instrument (UOP-1) shown in Fig. 17 has a 0.8-m modified Czerny-Turner mounting with an echelle grating (blaze angle 75°58′, 79 grooves/mm) and a 30° quartz prism for the cross dispersion. The reciprocal linear dispersion varies with wavelength from 0.031 nm/mm at 200 nm to 0.062 nm/mm at 400 nm. A quartz refractor plate for wavelength modulation is placed behind the entrance slit. The wavelength of the

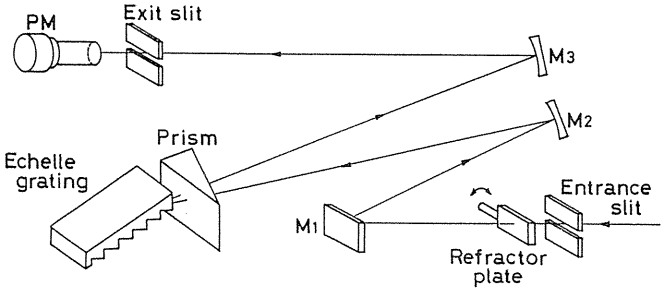

Fig. 17. Schematic diagram of the echelle spectrometer with crossed dispersion.

spectrometer is controlled by a computer, *i.e.*, the echelle and prism are rotated appropriately by a stepping motor when a wavelength is entered from the keyboard. This spectrometer designed for ICP-AES was evaluated in the point of view of the optical characteristics.[25)]

Since two-dimensional spectra are obtained with a cross-dispersed spectrometer, interference of the neighboring order was examined for different slit heights. Background shift by the interference of the Hg 546.1 nm line indicated that the entrance slit height of more than 0.5 mm interfered with the neighboring order. The increase of background by 0.1 % of the line intensity was found even with the slit height of less than 0.5 mm. The latter interference is not caused by the overlap of the order but by the scattered light from the strong spectral line in the neighboring order.

The grating efficiency in a free spectral range was measured by using a continuum light source, a deuterium lamp, at several different orders. The theory shows that the efficiency is described by the function,

$$I = A\{(\sin\theta) / \theta\}^2 \tag{19}$$

where, A is a constant and θ is the parameter related with wavelength. Experimental results could be fitted quite well with this theoretical curve. The efficiency of the grating at both end of the free spectral range is about 41 % of that at the center of the range.

Stray light of the spectrometer was examined by measuring the profiles of the Hg 253.61 nm line with the echelle spectrometer described above and also with a 1-m monochromator (Seiko SPS-1100H) with a holographic grating of 3600 grooves/mm for comparison. The results showed that there was no essential difference in the stray light levels for both spectrometers.

In order to examine the resolution of the echelle spectrometer, the interference of the Cu II 213. 598 nm line with the P I 213.618 nm was observed in ICP-AES.[26] These two lines were completely resolved with the echelle spectrometer but not with a spectrometer with medium resolution when the concentrations of copper and phosphorus were comparable. With the echelle spectrometer, however, the wing of the copper line was found to interfere with the phosphorus line when the copper concentration was very high, 500 μg/ml. In this case, the error in the determination is inevitable unless suitable background correction is applied. The background correction can be automatically performed with the wavelength modulation and 2nd derivative spectrometry in the present system, but a small signal suppression effect was observed when the copper concentration was 50 times larger than that of phosphorus.

4. 3 Application of Photodiode Array Detector

Photodiode array detectors can provide several hundred independent optical channels in the linear mode. These detectors, when interfaced on-line to a computer, will provide a great flexibility in spectrometry, including signal processing, scan rate selection, data accumulation and real-time display.

A self-scanning linear photodiode array of 512 channels (National, MEL-512KV) was mounted at the focal plan of a 25-cm monochromator (Nikon, P-250, grating 1200 grooves/mm, reciprocal linear dispersion 3 nm/mm) by replacing the exit slit and photomultiplier housing.[27] The photodiode array consists of 512 photodiode elements (16 μm × 464 μm) arranged at a distance of 12 μm between them. It is capable to measure over a 40 nm region at a time in the wavelength range from 200 to 900 nm. The data from the detector was acquired by a microcomputer and the spectrum was displayed on a CRT or a strip-chart recorder. The software for the signal acquisition and data processing was developed in our laboratory with an assembler language.[28]

The signal-to-dark current ratios were measured by using continuum light sources, a deuterium lamp below 360 nm and a tungsten lamp above 360 nm. A UV-cut filter was used above 650 nm to avoid the interference from the second order spectrum. For comparison, signal-to-dark current ratios were measured also with a photomultiplier (R-106) as detector. The signal-to-dark current ratio of the photodiode array detector was more than 100 times less than that of the photomultiplier below the wavelength range of 400 nm. Although the dark current of the photodiode can be reduced by cooling the element, present experiments was carried out at a room temperature.

In spite of the less signal-to-dark current ratio than that of the photomultiplier, the photodiode array detector is useful when spectra must be measured rapidly as in such a case as chromatography. Another interesting application is the measurement of the spatial distribution of spectral intensities by mounting the photodiode array along the slit length. Some of the results of the measurement of the axial distribution of spectral intensity in ICP-AES was already described in Section 3.3.

4. 4 Application of Image Dissector

The image dissector (ID) is basically a photomultiplier tube in which a field of view is electronically scanned across a small aperture. The ID tube employed in this experiments[29] is the one made by Hamamatsu Photonix Co. (R623) and its schematic diagram is shown in Fig. 18. A rectangular aperture (17 μm × 3 mm) was used to match the spectral line image replacing the standard 50 μm pinhole aperture. The deflection coil was driven by a home made current source (5 V, 300 mA). The ID tube was attached at the focal plane of a monochromator (Nikon, P-250) to investigate its characteristics as detector for emission spectrometry.

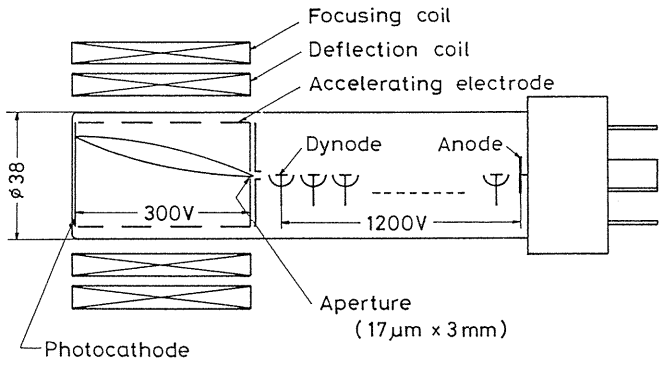

Fig. 18. Schematic diagram of an image dissector tube, R623.

The accelerating voltage was fixed at 300 V and the signal-to-dark current ratio was measured as a function of dynode voltage. The ratio was highest at 1100 V of the dynode voltage but 1200 V was used for the higher signal intensity. By using a deuterium lamp (200 − 400 nm) and a tungsten lamp (400 − 600 nm), the sensitivity of the ID was compared with that of the photomultiplier (Hamamatsu, R106). The high voltage for the photomultiplier was 800 V and the entrance slit of the monochromator was 20 μm × 3 mm for both of the detectors. The dark current level was 3.0×10^{-11} A for both detectors but the sensitivity of the ID was about one order of magnitude less than that of the photomultiplier.

Although the sensitivity of the ID as detector for AES was disappointing, it has quite desirable capabilities of extremely high scan rate, easy random access and high resolution. Therefore, the ID was again evaluated for the performance in ICP-AES.[30] The spectrometer used was a 1-m grating spectrograph (Shimadzu, GE-100). The 25-cm plate holder of the spectrograph was removed and the ID was attached at the center of the focal plan. Since the ID has no integration capability, the signal was stored in a transient memory and signal averager.

Another possibility of the measuring mode is the phase sensitive amplification with wavelength modulation.[30] The wavelength modulation can be performed by repetitive scanning over a small wavelength range around a line of interest. Automatic background correction can be obtained with this mode, though the capability of simultaneous multielement measurement is lost. The detection limits of various elements in ICP-AES were measured both with the digital averaging mode and wavelength modulation mode but the results with both of the mode were worse about a factor of 10 than the conventional method with a photomultiplier.

5. Water-Cooled Torch and Spray Chamber

5. 1 Development of Water-Cooled Torch

One of the disadvantages in the use of the ICP is the large consumption of argon gas. Typically, 10—20 l/min of argon flows are required for the total of outer, intermediate and carrier gases. Several authors proposed various torches such as mini-, air-cooled and water-cooled torches to reduce the argon consumption. Although these torches succeeded to reduce the argon consumption to some degree, they had also some inconveniences such as complexity of design, lower sensitivity and higher matrix effect.

Examples of the water-cooled torch we constructed are shown in Fig. 19.[31] A water flow of 2.5 l/min was used to cool the torch for the RF power from 1 to 1.8 kW. With the design in Fig. 19a, the plasma was easily initiated at 4 l/min of the outer gas when the carrier gas was not introduced. The plasma became unstable, however, when the carrier gas was introduced. By attaching a silica collar tube on top of the water jacket as shown in Fig. 19b, the plasma became more stable though the carrier gas flow rate was limited up to 0.5 l/min. With the torch shown in Fig. 19c, the plasma was initiated at about 5 l/min of the outer gas, and the latter can be reduced down to 2 l/min after the introduction of the carrier gas. With the

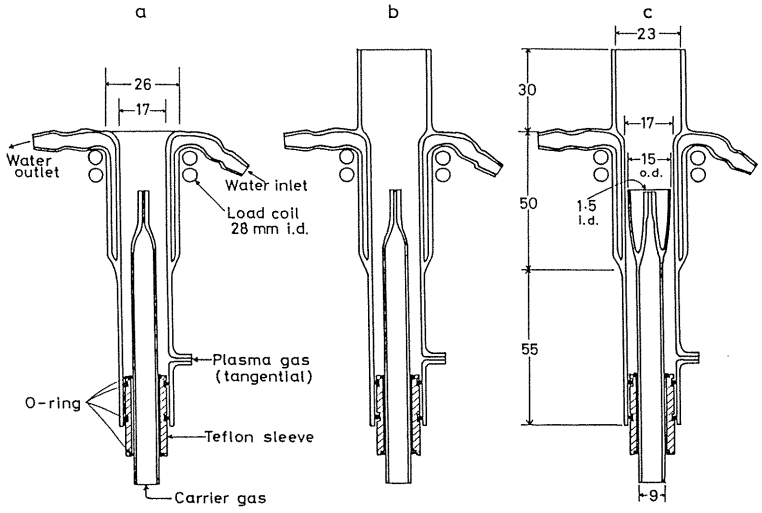

Fig. 19. Water-cooled torches for the low-flow ICP.

torch in Fig. 19c, the detection limits of many elements were determined at the total argon flow of 4.8 l/min including 0.8 l/min of the carrier gas and the RF power of 1.1 kW. These values are almost comparable to those with the conventional torch. The extension tube, however, was often degraded by the alkali solutions and had to be exchanged with new one.

A torch shown in Fig. 20 was designed[32] to overcome the inconvenience described above. The extension tube was found to be unnecessary when a commercial RF generator stabilized with a negative-feedback circuit was used. The torch can be easily constructed by modifying a conventional three-tube torch; the outer tube of the latter was removed by cutting at 5.5 cm below the top, and instead of it, a silica water-jacket with 6-cm length and the same internal diameter as the removed tube was attached with an epoxy resin adhesive. This design is advantageous because even a damaged conventional torch can be used again as far

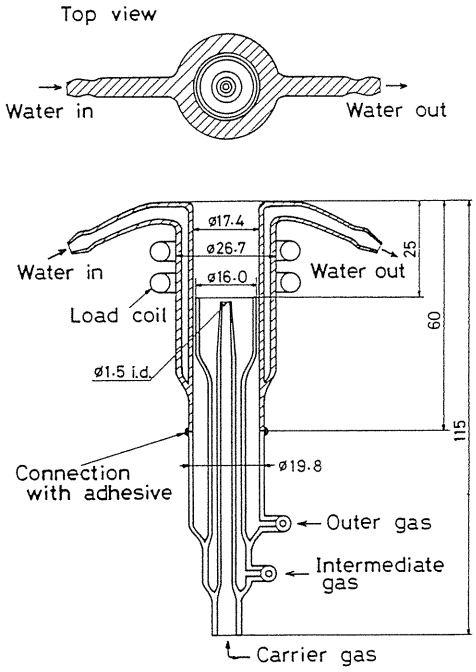

Fig. 20. Schematic drawing of the water-cooled torch.

as the damage is restricted to the outer tube. Since the inlet and outlet of the cooling water are located at the top of the jacket, air bubbles if formed in the jacket are rapidly carried away and do not cause the destruction of the jacket.

With the design of the torch in Fig. 20, the outer gas can be reduced down to 3 l/min before the plasma is extinguished and conveniently used at 4 l/min. As the outer gas flow rate decreases, the tail length of the plasma reduces because of the quenching action of entrained air. Axial emission profiles of ion and neutral calcium lines were measured with the facilities described in Section 3.1 at several different outer gas flow rates with the results shown in Fig. 21.[32] The intensities in the region below 10 mm above the load coil were not observed due to the shielding by the water jacket. As the outer gas flow rate is decreased, the

peak of the Ca II line emission shifts downward and the profiles become narrower and higher. At 4 l/min of the outer gas, the peak is located at 12—13 mm above the load coil and just above the water jacket. The position was found to be the optimum observation height also for other elements.

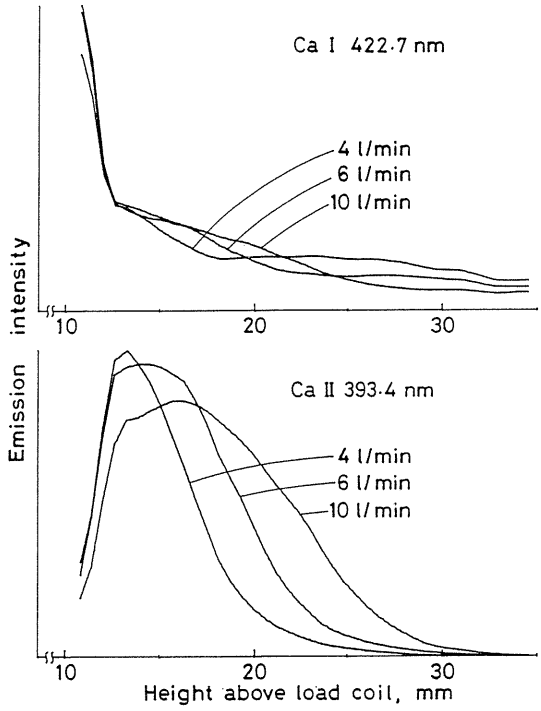

Fig. 21. Effect of outer gas flow rate on emission profiles of the Ca I 422.7 nm and Ca II 393.4 nm lines.

The axial temperature of the plasma was also highest at this observation height and comparable to that with the conventional torch. The interference effect of the concomitant elements was minimum at this observation height and almost the same with the conventional torch. The detection limits of many elements with the present water-cooled torch are also superior to or at the same level of those with the conventional torch. The total argon consumption with this torch is 5 l/min, less than 1/3 of that with the conventional torch.

5. 2 Axially Viewed ICP with Water-Cooled Torch

In ICP-AES, the plasma axis is generally arranged vertically and it is observed from the horizontal direction. Since sample aerosols are introduced into the central hole of the plasma and most of the spectral lines of the analytes are emitted strongly along the axis of the plasma, axial observation of the emission may enhance the measured intensities and, therefore, the sensitivity. Several authors already tried the axial observation of the plasma using a conventional torch and reported up to 10 times enhancement of the sensitivity.

Using the conventional torch, however, the tail flame of the plasma extends 15 to 20 cm from the end of the torch and reaches optical lens system unless the tail flame is extinguished by the strong air flow from the side of the flame. When a water-cooled torch is employed, not only the argon gas flows can be reduced but the length of the tail flame can be reduced.

The water-cooled torch constructed in this experiment is shown in Fig. 22.[33] The water jacket is extended *ca.* 30 mm longer than the torch described in Section 5.1 to reduce the entrainment of air and also to reduce the fluctuation of the tail flame. Under the conditions of the flow rates of outer gas 4.5, intermediate gas 0.5 and carrier gas 0.7 l/min and RF power of 1.3 kW, only a short tail flame was observed from the top end of the water jacket and a bare hand can be placed at a 10 cm distance without harm.

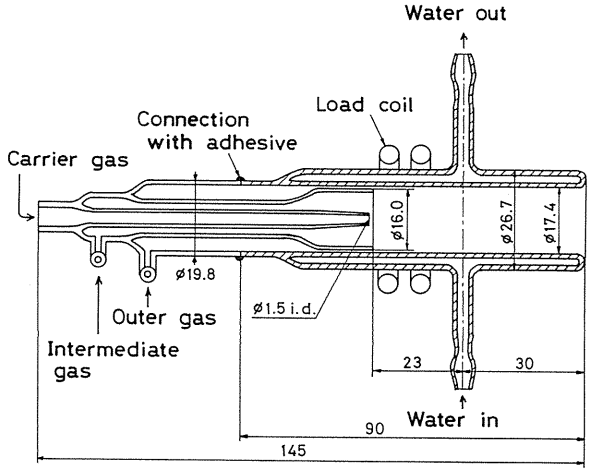

Fig. 22. Water-cooled torch for axially viewed ICP.

Radial intensity distribution of various lines has a bell shape indicating the strongest emission at the axis of the plasma.[33] The distribution of background measured at 422 nm, on the other hand, showed a minimum at the central axis. These results suggest that the axially viewed ICP effectively increases the signal-to-background ratio (SBR) and the sensitivity. Actually, detection limits measured with the present torch for many elements were 2 to 4 times superior to those with the conventional side view.

5. 3 Low-Memory Spray Chamber

In ICP-AES, a spray chamber has important roles that it removes relatively large droplets from the aerosol generated by a pneumatic nebulizer and mixes the resulted fine particle aerosol homogeneously with carrier gas before introducing the aerosol into the plasma. Most of the commercial instruments are equipped with a double-barrel type spray camber which is often called Scott-type chamber. When the sample is changed, the spray chamber is flushed by a pure water aerosol to remove the memory of the previous sample. In order to remove the memories completely, it usually needs several min which causes to reduce the throughput in routine analysis.

To reduce the flushing time, a spray chamber with low memory effect was designed[34] and shown in Fig. 23. The chamber has a cone-shape and a volume of 52 ml which is about half of that of the Scott-type chamber. The larger chambers with 138 and 200 ml of the volume were tried but less satisfactory. The smaller the volume becomes the memory effect smaller, but signal fluctuation larger. A commercial glass concentric nebulizer (Meinhard type) and a glass spoiler were positioned at the bottom of the chamber with a distance of 4—6 mm between them. Since the gas flow rate inside the chamber is lowest near the bottom of the chamber, the large droplets are efficiently removed to the drain.

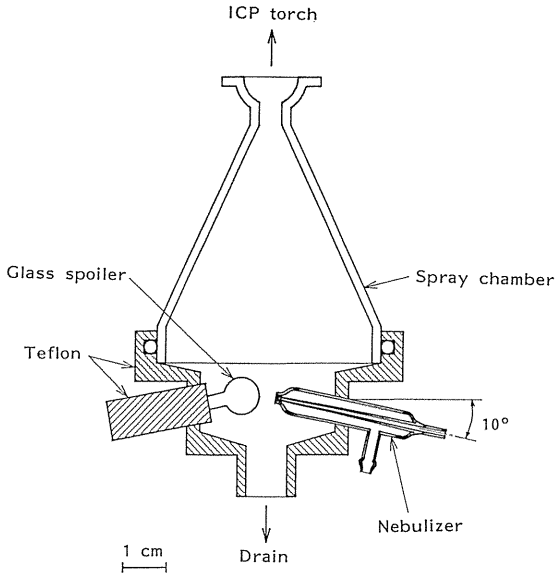

Fig. 23. Schematic diagram of the cone-type glass spray chamber.

The memory effect was compared with the Scott-type chamber by observing the decrease in the intensity of the Mn II 257.6 nm line after the sample solution containing 1000 μg/ml of Mn was changed to pure water. The intensity was measured in every 30 s with the integration time of 1 s. The time necessary to decrease the Mn line intensity to 10^{-4} of the initial intensity (1000 μg/ml) was 40—50 s for cone-type spray chamber while 2—2.5 min for Scott-type chamber. This means the necessary flushing time of the cone-type spray chamber can be reduced to about 1/3 of the Scott-type chamber.

The nebulization efficiency was also increased from 1.4 % for Scott-type chamber to 2.0 % for cone-type chamber. This increase reflected to the increase in the signal-to-background ratio for many lines by a factor of about 2 to 4. The detection limits are also improved.

6. Sample Introduction to Plasma for Emission Spectrometry

6. 1 Methodology of Sample Introduction

The sample introduction process largely determines the accuracy and precision of the determination in analytical atomic spectroscopy. Therefore, a large number of research works on the sample introduction into the ICP have been published. Selection of the best sample introduction procedure for an analysis requires consideration of a number of points. These include:

1) the type of sample (solid, liquid, gas),
2) the concentration levels, and also the range of the levels for the elements to be determined,
3) the accuracy required,
4) the precision required,
5) the amount of material available,
6) the number of determinations required per hour,
7) special requirements, such as whether speciation information is needed.

Although the ICP-AES was first developed as a technique for the solution analysis using a pneumatic nebulizer, various types of samples can be analyzed under the consideration described above. In the analysis of solutions, microliter sample introduction technique is often necessary *e.g.*, when the trace elements in pure materials are separated and concentrated in a small amount of solutions. Laser ablation technique is useful for the direct analysis of solid samples especially when the samples are difficult to be decomposed. Finally, a method for direct particle analysis developed in our laboratory will be described in this chapter.

6. 2 Microliter Sample Introduction

6. 2. 1 Flow Injection Technique

Conventional sample introduction technique with a pneumatic nebulizer requires at least several ml of sample solution, because the sample uptake rate is usually 3—4 ml/min and continuous nebulization for 30—40 s is required for the stabilization and integration of signals. The amount of the sample available is some times limited to less than 1 ml such as biological fluids and trace element concentrates.

Flow injection analysis in which sample plugs are injected into a flow of carrier stream has been increasingly used in various analytical problem solutions. The application of it to ICP-AES was first attempted in our laboratory.[35] A simple apparatus for flow injection is shown in Fig. 24. A "T"-shape line sample injector was made by pyrex glass of 1-mm i.d. and a silicone septum for the injection of samples with a micro-syringe. The injector was connected to a conventional nebulizer with Teflon tube through a spray chamber of a volume of 35 ml. Pure water was used as a carrier stream.

In flow injection technique, sample plugs are not usually separated from carrier stream by the air segmentation. For microsamples, however, the dilution effect was found to reduce the signal peak height and broaden the peak width. The segmentation of sample plugs with small air bubbles removed these difficulties. The inlet of the carrier water was raised above the water surface for a short time to introduce an air bubble and sample solution was injected into this air bubble when the bubble reached the injection port as shown in the circle in Fig. 24. The optimum sample uptake rate was 1.3 ml/min for 40 μl samples. The peak heights of signals under these conditions were about 65 % of those for the continuous nebulization. Matrix effect was considerably less than that for continuous neblization; the same suppression

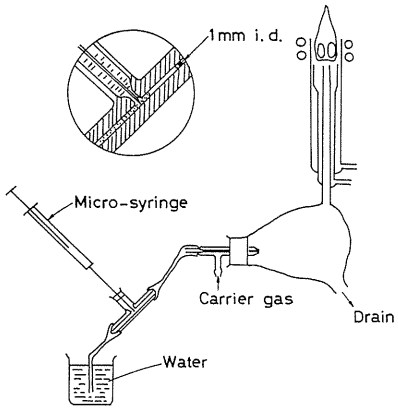

Fig. 24. Nebulization system and plasma torch for flow injection.

effect of potassium on the signal of Cr and B was observed only at 10 times higher concentration of the matrix than in continuous nebulization.

The sample injection into the air bubble described above required somewhat skills and the reproducibility depended on the operator. A semi-automatic microliter sample injection method was developed to overcome this problem.[36] The schematic diagram of the sample introduction system is shown in Fig. 25. A line sample injector and an 8-way motor-driven rotary valve for gas chromatography were used. The operation of the sample introduction was carried out as follows, where the step numbers correspond to the position of the 8-way valve.

1) The pathway from the valve to the nebulizer is flushed with argon, 2) the argon flow is stopped and a 40-μl sample is manually injected into the line sample injector through a silicone septum with a micro-syringe, 3) argon carries the sample gently to the nebulizer, 4) water is introduced from the valve into the nebulizer to rinse the sample pathway. The steps 1–4 are repeated at the valve positions 5–8. By pushing the "Reset" button, the step proceeds to step 2 or 6 to accept the sample. After the sample is injected and by pushing the "Start" button, the following sequence starts automatically.

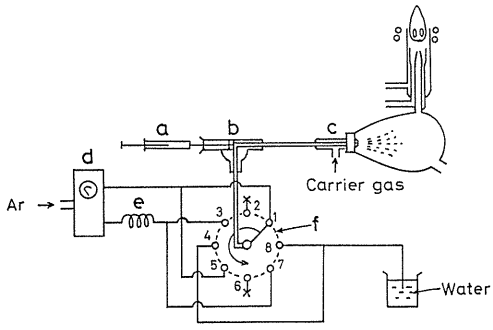

Fig. 25. Schematic diagram of semi-automatic microsample injector. a: micro-syringe, b: line sample injector, c: concentric nebulizer, d: gas regulator, e: stainless steel capillary, f: 8-way valve.

Emission responses of the Zr II 343.8 nm line at 1 μg/ml for a number of repeated injections are shown in Fig. 26. The relative standard deviation of the peak height was 1.7 %, which was considerably improved compared to the manual introduction into the air bubble. Although the detection limits of the elements by the present method are worse by a factor of 2–6 compared with the continuous nebulization, the amount of sample solution required is only 40 μl compared with several ml for the continuous nebulization.

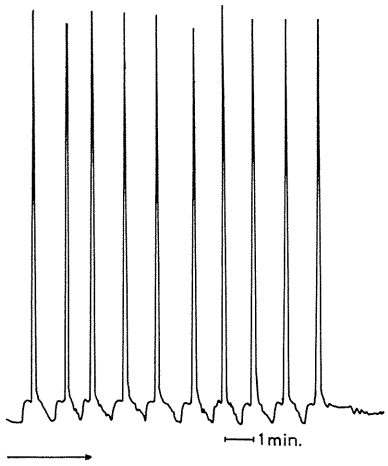

Fig. 26. Reproducibility of the peak height of the Zr II 343.8 nm line for the 40-μl sample injection. Zr: 1 μg/ml.

6. 2. 2 *Application to Trace Analysis*

One of the challenging problems in steel analysis is the determination of traces of rare earth elements, because only trace amounts of rare earths are contained in ordinary steel samples and iron lines interfere with the lines of rare earths unless iron is removed completely. When rare earth elements are separated and concentrated in a small volume of solution, the microliter sample injection technique described above will become a good choice for the determination of them by ICP-AES.[37)]

After 1 g of carbon steel sample is dissolved by hydrochloric and nitric acid, the solution is heated to dryness. The residue is dissolved again in 25 ml of (1+1) hydrochloric acid. Iron in the solution is extracted 2 times with 25 ml of MIBK and the aqueous phase is transferred to a beaker and heated to dryness. The residue is dissolved in 1.0 ml of (1+10) hydrochloric acid for the ICP-AES.

The detection limits of the method were La 0.01, Ce 0.2, Pr 0.2, Nd 0.2, Sm 0.2 and Eu 0.03 μg/ml and these values correspond to the detection limits in steel at μg/g. Analytical results for various samples showed that the detection limits were not enough to analyze real samples though only La was detected (0.12 μg/g) in a carbon steel sample of Japan Standards of Iron and Steel, JSS 050-1.

6. 3 *Ultrasonic Nebulizer for Microliter Samples*

The most common method for introducing samples into an ICP is the pneumatic nebulization of solutions. Although ultrasonic nebulizers were extensively studied in the early stage of the development of the ICP-AES, they were gradually replaced by pneumatic nebulizer mainly due to cumbersome operation procedures and less stability. In 1970s, we also constructed an ultrasonic nebulizer[38] for atomic spectrometry of solutions and successfully applied to the arc excitation of solutions.[39]

There have been reported various types of the ultrasonic nebulizer which usually needs at least several ml of sample solutions. As described in Section 6.2, microliter sample nebulizer is often desirable in trace analysis. In Fig. 27, a schematic diagram of the ultrasonic nebulizer is shown which was designed for microliter samples in ICP-AES.[40] The sample cell is made of a glass tube (11.5 mm i.d., 25 mm long) with a thin bottom plate made from microscope cover glass (0.15 mm thick). Two sample cells are mounted in a sliding cell holder so that they are rapidly exchanged without disturbing the nebulization. The ultrasonic power of 1.72 MHz is coupled to the sample cell through cooling water.

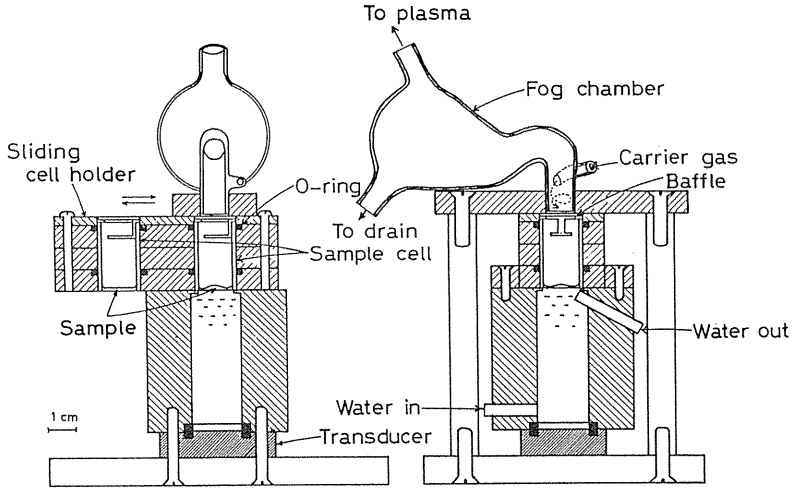

Fig. 27. Schematic diagram of the ultrasonic nebulizer for microliter samples.

A 35-ml fog chamber is designed so that the drain will not return to the sample cell. The aerosol was introduced into the ICP without desolvation. The efficiency of the nebulizer is highest at the sample volume of 300 μl. In spite of the much smaller sample consumption, the signal intensity with the ultrasonic nebulizer is several times higher than that with the pneumatic nebulizer. The aerosol can be generated for more than 60 s with a 300-μl sample, so that a conventional signal integrator can be used without modification.

The signal, however, is not as stable as with the pneumatic nebulizer and internal standard method is necessary for the measurements with better precision. Effect of the acid concentration was also found more serious than with the pneumatic nebulizer, especially for sulfuric acid. Signal depression effect was observed even by 0.1 % of sulfuric acid with the ultrasonic nebulizer, while it appeared by 3 % with the pneumatic nebulizer.

6. 4 Electrothermal Vaporization

Electrothermal vaporization is one of the most popular sample introduction techniques in both AAS and AES. Various vaporizers including graphite furnace, metal filament and boat are commonly utilized. In AAS, the graphite furnace serves as the atom cell as well as the sample atomization cell. In AES, on the other hand, the electrothermal vaporizer serves only as the sample atomizer independent to the excitation source.

Metal filament atomizers are suited especially for microliter sample introduction, because only several μl of solution is required to deposit it on the filament. A tantalum filament vaporizer was successfully used for the determination of picogram of metals in metalloenzyme[41] in microwave induced helium plasma emission spectrometry, in which the filament was heated by a discharge current of a high-capacity condenser. The latter technique is quite effective because the heating rate of the filament is very rapid compared to the heating by a continuous current.[42]

In ICP-AES, a V-shape tungsten filament made of 0.2 mm dia. and 18 mm long wire, was used as shown in Fig. 28.[43] A small vaporization chamber with a volume of *ca.* 1 ml was connected to a torch with a Teflon tube of 1-mm i.d. After 10 μl of sample solution is deposited on the filament, the solvent is evaporated by heating the filament with a current of 3.2–3.6 A. The filament is then heated by a discharge current of a capacitor of 0.22 F which is charged at an appropriate voltage of 6.25–8.5 V. The maximum temperature of the filament was 1000, 1200 and 1500°C at the charging voltage of 6, 7 and 8 V, respectively. The optimum charging voltage was dependent on the element to be determined; 6.25 V for zinc, 8.5 V for vanadium and 7.75 V for other elements. Signal peaks appears within 0.2 s after the start of the heating.

The detection limits of various elements by the present method are better than the reported values by more than one or two orders of magnitude. This is chiefly due to the exceptionally small dead space adopted in this system. In the electrothermal vaporization method, the effect of matrix is also important. Matrix modification or matrix matching is usually necessary when the complex samples are analyzed.

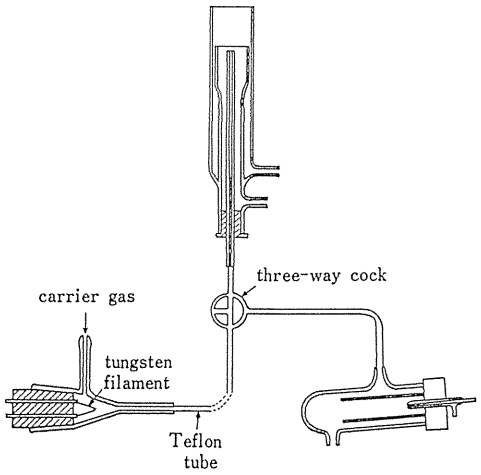

Fig. 28. Schematic diagram of evaporation chamber and torch.

6. 5 *Laser Ablation*

Laser vaporization has long been used in emission spectrometry as a micro-sampling technique of solid samples. In laser microprobe analysis, a sample vapor produced by a laser pulse is usually excited again by a spark source, because the laser plume generated by a high-power laser shot has a spectrum of intense background and self absorption. Therefore, the method is subject to instabilities of both the laser pulse and the excitation source. Since the ICP is a quite stable source as described before, laser ablation-ICP emission spectrometry has a potential ability of high-precision microprobe analysis.

Although there have been a number of reports on laser ablation-ICP emission spectrometry, they usually employ lasers with output power of more than 1 J. A low-power laser, however, has a possibility to be used in the ICP excitation because the ICP can effectively excite sample vapors introduced into it. In this experiment[44], a normal pulse Nd: YAG laser of 0.1 J was examined for the practical analysis.

A schematic diagram of laser optics is shown in Fig. 29. An image of the sample surface was magnified about 100-fold on a monitoring TV screen. An acrylic resin plate of 10 mm thick with an 8-mm hole in the center and covered with a microscope cover glass of 0.2 mm thick on the hole, was used as a sample chamber. A laser generator was an NEC Nd: YAG laser, SL129A, which generated laser pulse of 0.1 J in single pulse mode and 0.07 J at 10 pulse per second. The laser with the wavelength of 1.06 μm and pulse duration of *ca.* 100 μs, was focussed on the sample surface by a 20-mm focal length objective lens of a microscope.

At first, the amounts of metals vaporized by a single pulse of the laser were measured from the weight losses using a microbalance of Cahn model 26 which had a resolution of 0.1 μg at 5 mg. The results were compared with the data reported in a literature using a 1.0 J Nd-glass laser. There was a tendency that the larger the evaporation rate, the smaller the effect of the difference in laser energy. This is probably due to the greater reflection loss of laser energy on the metal surfaces for the low-energy laser, which produces smaller craters than the high-energy laser does.

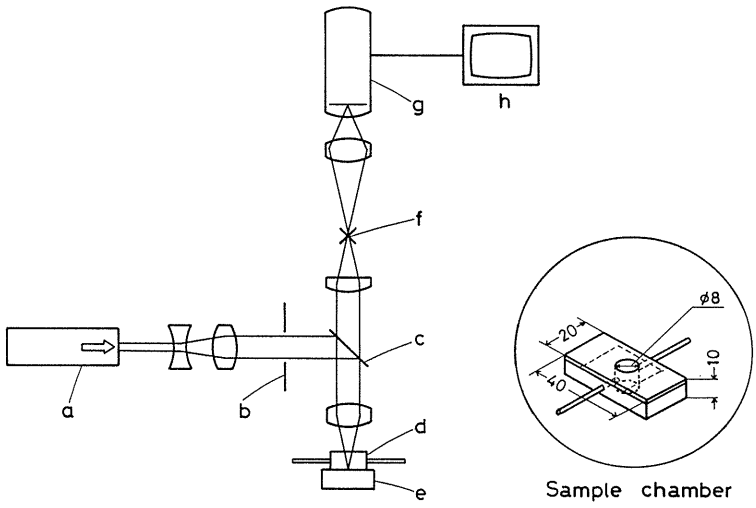

Fig. 29. Schematic diagram of laser optics. a: Nd: YAG laser, b: diaphragm, c: dichroic mirror, d: sample chamber, e: sample, f: cross-mark plate, g: TV camera, h: TV monitor.

The relative standard deviations of the intensities of Cr, Mn and Ni in case-hardening steel samples were 1.8–6.0 % in single pulse mode and 1.7–5.9 % in multi-pulse mode. The detection limits of these elements were Cr 0.017, Mn 0.074 and Ni 0.025 % in single pulse mode and Cr 0.004, Mn 0.047 and Ni 0.004 % in multi-pulse mode. Though the detection limits of these elements reported previously with a high-power laser are somewhat lower than the above results, the low-power laser ablation ICP-AES can also be conveniently used in the practical analysis.

6. 6 Direct Particle Analysis

6. 6. 1 Instrumentation

Chemical composition and size distribution of airborne particles are measured frequently in the study of environmental science and in the development of air pollution control technologies. Usually, particulate matter in air is collected on a membrane or glass fiber filter using a high volume or low volume sampler and the filter is subjected to chemical analysis. In these methods, however, a lengthy sampling time, often exceeding several hours, is required to collect sufficient amounts of particles. Moreover, time-consuming dissolution of collected samples is necessary for the analysis by the methods such as AAS and ICP-AES.

In this experiment[45], ICP-AES was investigated by directly introducing air samples into the ICP. Pulse-like emission signals from individual particles were measured with a pulse-height analyzer calibrated by using monodisperse aerosols of known composition. A block diagram of the instrumentation is shown in Fig. 30. Air samples were introduced into the plasma by the suction pressure of a conventional concentric nebulizer for liquid samples. Signals from the monochromator were passed through a preamplifier, a logarithmic amplifier and a low-pass filter before being introduced into the pulse-height analyzer, which was consisted of an analog-to-digital converter and a personal computer.

Monodisperse aerosols were generated by drying salt solution droplets of a uniform diameter produced by breaking a cylindrical liquid jet from an orifice attached to the head of an ultrasonic horn. The orifice diameter was *ca.* 18 μm and the frequency of the orifice vibration was 28.2 kHz. For example, when sodium chloride solutions containing 100, 50 and 10 μg Na/ml are fed at a rate of 48 μl/min, the generated liquid droplets have a diameter of

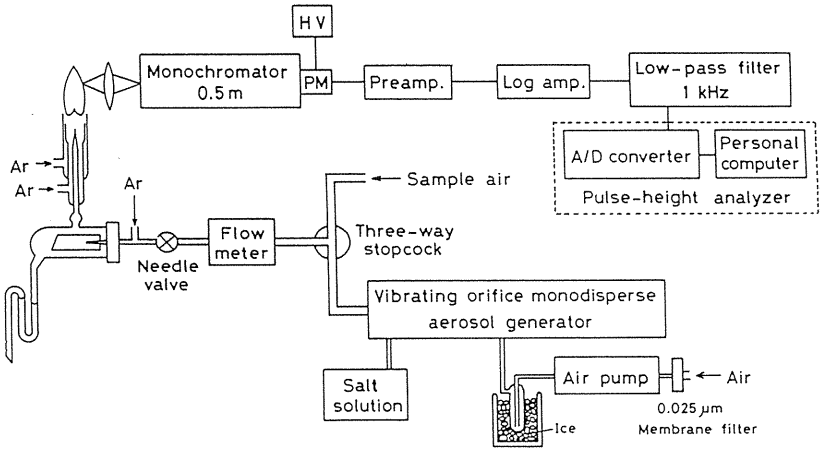

Fig. 30. Block diagram of particle analyzer by ICP-AES.

37.8 μm and the diameters of sodium chloride crystals after drying the droplets are 1.9, 1.5 and 0.9 μm, respectively, corresponding to the concentration of the solutions.

An example of the emission signal of the Ca II 393.36 nm line is shown in Fig. 31 when a monodisperse aerosol of calcium with a diameter of 1.9 μm was introduced into the ICP. Some strong pulses may be due to the emission of two particles simultaneously introduced into the plasma. Sharp pulse-height spectra were obtained from the monodisperse aerosols containing various metals by measuring the emission signals of these elements. Calibration curves for the relation between the channel number of the pulse height analyzer and the particle diameter were prepared by the monodisperse aerosols of the same element with different diameters. The detection limits of the present method for particle diameters were estimated to be 0.22 μm for Cu and 0.10 μm for Ca.

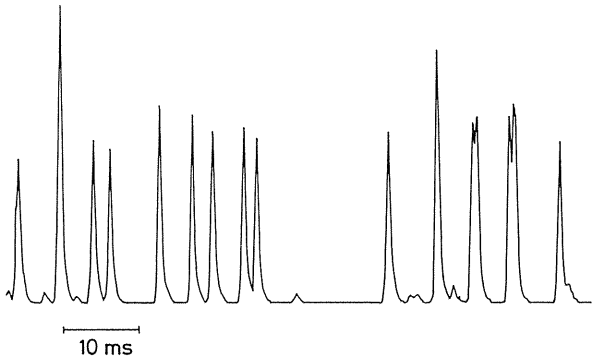

Fig. 31. Oscillogram of the calcium emission from the $CaCl_2$ monodisperse particles with a diameter of 1.9 μm.

6. 6. 2 Particle Number Density and Particle Diameter

For the aerosol particles with known composition, the particle number density can easily be determined by the method described in Section 6.6.1. The aerosol particle number density in a cylindrical container gradually decreases with time by the gravitational sedimentation at the bottom and deposition at the wall by the Brownian diffusion. Theoretically, the variation of particle number density, n, with time can be expressed by,

$$dn/dt = -n\{DS/(\delta V) + vS_1/V\} \tag{20}$$

where D is the diffusion coefficient, S the inside surface area of container, S_1 the area of the bottom, V the volume of the container, δ the thickness of the diffusion layer and v the final sedimentation speed of particles.

Using a cylindrical stainless steel container (21 cm high, 21 cm diameter, volume 7.0 l), the variation of the particle number density as a function of time was measured for various aerosols[46] by the particle analyzer based on ICP-AES. Aerosols were generated with various salt powders and they were sampled in every 3 to 5 min to measure the number densities. As is expected from Equ. 20, the graph of $\log(n)$ plotted against time showed a straight line.

The relation between the slope of the curve and the particle size can be derived theoretically from the Equ. 20. By using monodisperse aerosols of calcium acetate, the linear relation between the $d\log(n)/dt$ and the particle diameter was also confirmed experimentally. This relation is useful for the measurement of particle size distribution of known compounds.

6. 6. 3 Elemental Content and Size Measurement

The method described in Section 6.6.1 can only provide the distribution of the elemental quantities in aerosol particles but not the information of the particle size. Therefore, the particle size must be measured by other method for the determination of the elemental concentration. The particle size was tried to measure by the laser scattering cell incorporated in the aerosol introduction tubing.[47)]

The aerosol scattering cell was constructed by using a semiconductor laser of 2.7 mW output at 670 nm. The pulse-like scattered light from each particle was detected by a photomultiplier. The atomic emission pulses from the ICP are observed at some delay time after the scattered light pulses are observed. The correlation between the emission and scattered light pulses was carried out by a computer and displayed on a CRT. An example is shown in

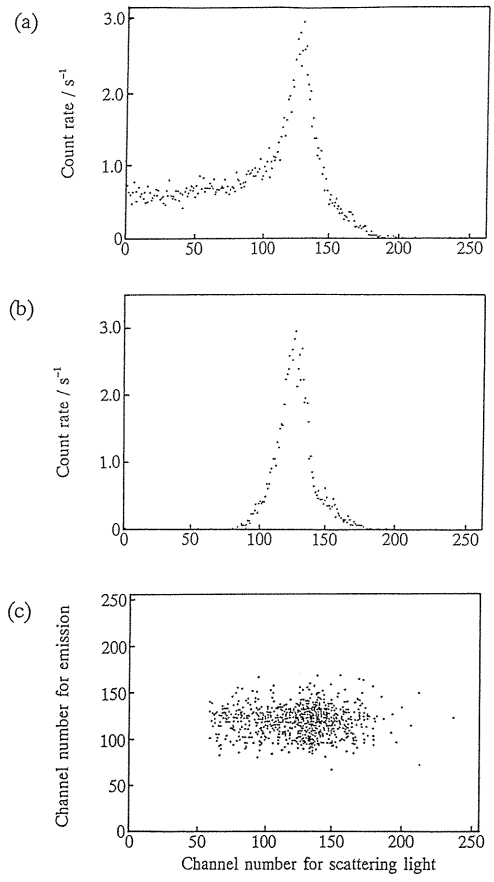

Fig. 32. a) Pulse-height spectrum of the laser light scattered signals, b) pulse-height spectrum of the emission signals and c) a plot of the corresponding pulse heights.

Fig. 32 for a monodisperse aerosol of calcium acetate with a particle diameter of 1.22 μm and calcium content of 2.92 pg. The plots in Fig. 32c should be concentrated in the center of the graph if the scattered light pulses are correlated correctly to the emission signals. Although the results in this experiment suggest the necessity for further improvement in the measuring system, the potential of the system is apparent for the simultaneous measurement of the elemental content and size of aerosol particles.

6. 6. 4 Application to Biological Cell Analysis

The airborne particle analyzer using ICP-AES was applied to the measurement of calcium content in dried individual biological cells in air.[48] Cell samples such as mouse fibroblast, human pancreas and human umbilical vein endothelial were carefully washed with a phosphate-buffered saline and sedimented by gravity. The cells were suspended again in 70 % ethanol and nebulized by a glass concentric nebulizer for the introduction into an ICP. The instruments similar to the one shown in Fig. 40 were used except that a 1-m monochromator, Seiko SPS-1100H (1-m holographic grating, 3600 grooves/mm), was used.

A calibration curve was prepared by using monodisperse aerosols of calcium acetate, containing 0.36, 0.11 and 0.036 pg of calcium in each particle. A linear relationship was obtained between the logarithms of calcium content and the channel number of the pulse-height analyzer. The mean value of calcium content in individual cells of mouse fibroblast cells was estimated to be 0.057 pg. Since the size of the cells ranged from 10 to 15 μm, the calcium concentration in the cell can be calculated to be in a range from 0.82 to 2.8 mM, assuming a spherical cell. The calculated value is close to the intracellular total calcium concentration, 1–2 mM, in a typical mammalian cell reported in the literature. Similarly, calcium contents of human pancreas and endothelium cells were determined to be 0.16 and 0.27 mM, respectively.

7. Inductively Coupled Plasma Mass Spectrometry

7. 1 Inductively Coupled Plasma as Ion Source

Since the pioneering work on ICP-MS was reported in 1980[4], the method has grown into a significant, new technique for trace element analysis and many reviews[49] and books[50] on this technique have already been published. In this technique, analyte ions generated in an ICP are extracted into a vacuum chamber and measured with a mass spectrometer. The ICP is an excellent source for atomic emission spectrometry as described in the previous sections. From the fact that most analysis in ICP-AES are performed by observing ion lines, analyte elements can be expected to be highly ionized in the ICP.

For the plasmas at thermal equilibrium conditions, the ionization of elements is governed by the Saha Equation,

$$N^{+}N_{e}/N = (2\pi mkT)^{3/2}/h^{3} \cdot (2Z^{+}/Z) \cdot \exp(-V/kT) \tag{21}$$

where N^{+}, N_e and N are the number densities of ions, electrons and atoms, respectively, m the electron mass, k the Boltzmann constant, T the temperature, h the Planck constant, Z^{+} and Z are the partition functions of ions and atoms, respectively, and V is the ionization potential. When the values of $N_e = 1.475 \times 10^{14}$ cm^{-3} and $T = 6680$ K are used, the ionization degrees, $N^{+}/(N+N^{+})$, calculated by the Equ. 21 are higher than 90 % for the elements with the ionization potential of less than 8 eV.

7. 2 Ion Extraction from Plasma

In 1983, we began to construct an ICP mass spectrometer with the collaboration of ULVAC Co., Japan. The first design was similar to the one reported by Houk *et al.*[4] with two-stage differential evacuation, but it was soon found to suffer from clogging by salt at the sampling orifice of 50 μm diameter. Therefore, three-stage differential pumping was finally adopted as shown in Fig. 33.[51]

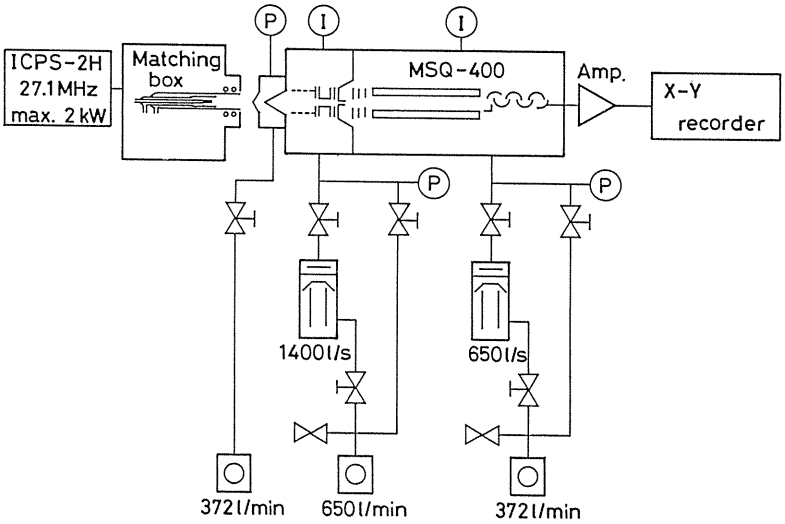

Fig. 33. Schematic diagram of ICP-mass spectrometer.

With this instrument, various characteristics of ICP-MS was measured such as background spectra for various acid solutions, effect of the sampling depth and effect of the carrier gas flow rate. As an example, effect of the carrier gas flow rate on the intensities of La^{+}, La^{2+} and their ratio is shown in Fig. 34.[51] The ratios of the doubly charged to singly charged ions of lanthanum were found to increase with the carrier gas flow rate. This phenomenon was later explained by the effect of the secondary discharge at the mouth of the sampling orifice which was caused by the capacitive coupling of RF power to the plasma.

In order to investigate the ion extraction behavior at the sampling orifice, the optical characteristics of an afterglow extracted from an inductively coupled plasma was measured.[52] A vacuum chamber consisting of a sampling orifice and a quartz cylinder was constructed to observe the afterglow. As shown in Fig. 35, a dark space of about 6 mm in diameter surrounded by a bright edge is clearly visible inside of the sampling orifice. The color of the dark space is pale blue and the edge is bluish red. A round bright spot is observed right above the dark space and the jet gradually darkens downstream.

The bright edge described above can be regarded as the shock wave known as the "barrel shock" in the supersonic molecular beam experiments, then the bright spot corresponds to the "Mach" disk and the dark space to the "zone of silence". The distance x_M between the orifice and the Mach disk was measured at various pressure p_1 inside the chamber. In the

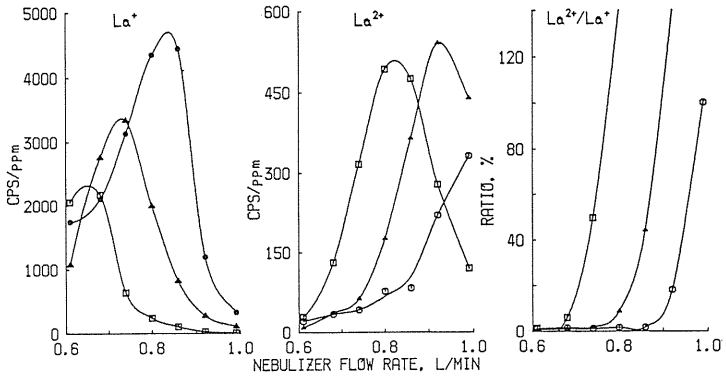

Fig. 34. Effect of the carrier gas flow rate on the ion intensities.

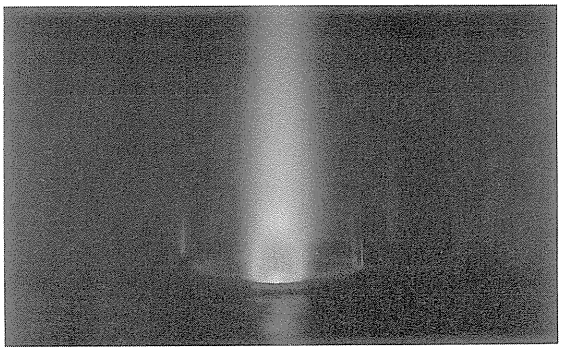

Fig. 35. Photograph of the shock wave in the extracted afterglow.

molecular beam experiments, x_M is known to be expressed as,

$$x_M = 0.67\ D(p_0\ /\ p_1)^{1/2} \tag{22}$$

where D is the orifice diameter and p_0 is pressure outside of the orifice, *i.e.*, 760 Torr. The experimental results were found to fit well with the Equ. 22, which shows that the equation derived from the cold neutral gases can be extended to the high temperature ionized gases.

In the early stage of the development of an ICP-MS instrument, relatively strong continuum background was observed in the mass spectra. Since the detection capability of the method is limited by the signal-to-background ratio (SBR), it is important to reduce the background. The most significant effect on the continuum was found to be the diameter of the optical baffle plate located in the ion lens.[53] Since the ion detector is also sensitive to light in the vacuum ultraviolet region, the strong emission light from the plasma must be stopped by the optical baffle plate. The larger is the diameter of the plate, the further the

background reduced but the analyte signal also reduced, and the largest signal-to-noise ratio (SNR) was obtained with the diameter of 6 mm.

The continuum background was also affected by various instrumental conditions such as sampling depth, lens voltage and ion deflector voltage. Since the ICP operating conditions for the best SBR does not necessarily coincide with the conditions for the least interference by oxide and doubly charged ions, compromised conditions must be chosen depending on the analytical problems.

7. 3 Non-Spectroscopic Matrix Effect

The analyte signals in ICP-MS are influenced not only by the operating parameters of the instrument but also by the presence of concomitant elements. The effect can be classified into non-spectroscopic and spectroscopic interferences. The latter consist of isobaric interferences and spectral overlaps with doubly charged ions and polyatomic ions such as oxide and hydroxide ions of concomitant elements. Non-spectroscopic interferences cause suppression of analyte signals in most cases and enhancement in a few cases in the presence of matrix elements. Generally, these non-spectroscopic interferences, *i.e.* matrix effects, are more severe than those in ICP-AES.

In Fig. 36, the effect of various matrix elements shown at the top of the figure on the intensities of analytes, Co, Y, La and Bi.[54] The suppression effect obviously increases with increasing atomic weight of matrix elements. The suppression effect, on the other hand, becomes less significant with increasing atomic weight of analyte. These results were also confirmed by the experiments with a commercial instruments in our laboratory[55] and other researchers.

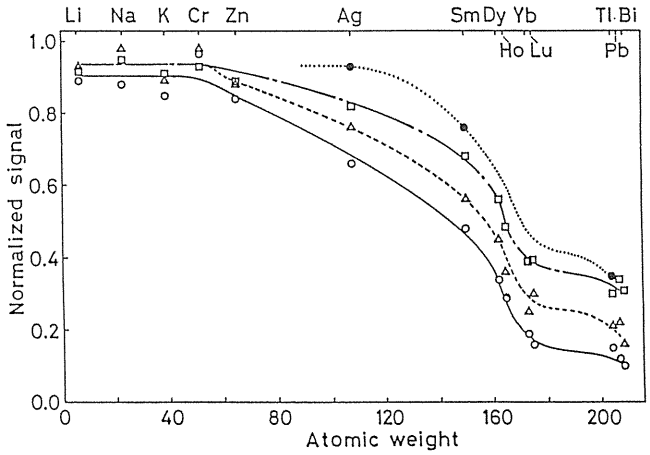

Fig. 36. Variation of suppression effect as a function of atomic weight of matrix elements. Analyte: ○ Co, △ Y, □ La, ● Bi, 10^{-5} M. Matrix: 0.01 M.

Although several investigations have tried to explain the mechanism of the matrix effect in ICP-MS, any conclusive explanation has not yet been developed, probably because several mechanisms may involved. The most important cause is now believed to be the space charge effect in ion lens system.

7. 4 *Nitrogen, Oxygen and Reduced Pressure ICP-MS*

Spectral interferences resulting from Ar adduct ions such as ArH^+, ArO^+ and Ar_2^+ in ICP-MS are unavoidable unless the supporting gas is replaced by other gases. The generation of N_2 or O_2 plasma, however, is considerably difficult with a conventional RF generator of an output power of less than 2 kW. By modifying the commercial matching circuit, Ar of the outer and carrier gases became to be replaced by pure N_2 or O_2 at an RF power of 1.8 kW[56], though Ar of the intermediate gas could not be replaced.

Since Ar is still used for the intermediate gas, polyatomic ions such as ArO^+ and Ar^{2+} could not be removed in N_2 or O_2 ICP-MS. Detection limits of elements with O_2 plasma, however, were superior to Ar plasma for the elements with relatively low ionization potential such as Cs, Ba and La. The more important feature of the O_2 plasma is the capability of the introduction of organic solvents into the plasma, because the carbon deposition at the sampling orifice can be completely avoided.

In ICP-MS with an Ar plasma, detection limits generally deteriorate with increasing ionization potential of the elements. Several authors have investigated He ICP or He MIP (microwave induced plasma) to improve the sensitivity for the elements with high ionization potential. Another approach for the same purpose may be the employment of a reduced pressure ICP. Since the LTE conditions seldom exist in the plasma at reduced pressure, the sensitivity of the elements with high ionization potential could possibly be improved as a result of the energy transfer from the high kinetic energy electrons.

The reduced pressure ICP-MS with Ar was investigated for the determination of iodine.[57] The sampling orifice of a conventional ICP mass spectrometer was removed and a new orifice and vacuum fitted water-cooled torch was attached. Saturated iodine vapor as analyte was introduced into the ICP by a peristaltic pump. A preliminary examination showed that the sensitivity increased more than an order of magnitude compared to the atmospheric Ar ICP.

7. 5 *Application of Water-Cooled Torch*

Although a large number of works have been carried out for the torch in ICP-AES, only a limited number of investigations were reported to find an ideal torch for ICP-MS.[58] Water-cooled torches in ICP-AES are successful to reduce the Ar consumption as described in Chapter 5 and they may also be used in ICP-MS.

In the preliminary experiments[59], the sensitivity was found to decrease by 40 to 50 % with the use of the water-cooled torch. Copper ions originated from the sampling orifice, on the other hand, were about 10 times stronger than those with the conventional torch. These results suggest that the enhanced secondary discharge occurs at the sampling orifice by the use of the water-cooled torch. Since the secondary discharge at the sampling orifice is known to be caused by the capacitive coupling of RF power to the plasma, the electrostatic shielding of the torch was studied.

A thin copper plate was inserted in the water jacket inside of the load coil and the plate was grounded after the plasma ignition.[60] With the electrostatic shielding, the plasma dc potential induced by the capacitive RF coupling was found to be completely eliminated. Consequently, the secondary discharge at the sampling orifice disappeared and Cu^+ signal became negligibly small. Moreover, the signals of analyte ions increased and doubly charged ions decreased even compared to those with the conventional torch. It was also found that the intensities of ArO^+ and Ar_2^+ decreased with the electrostatic shielding. In the several recent commercial instruments, the electrostatic shielding of the torch is adopted in ICP-MS to reduce such ions.

7. 6 Direct Particle Analysis by ICP-MS

Direct introduction of particles into the ICP for the determination of elemental contents by ICP-AES was already described in Section 6.6. Although the method is capable to determine the contents of major elements in the particles larger than 0.1 μm in diameter, sensitivity is not enough for the determination of minor elements especially in biological cells. In order to increase the sensitivity, direct introduction of aerosol particles into the plasma was tried in ICP-MS.[61)]

The output signals from the ion detector were amplified by a preamplifier with a relatively long time constant of 0.33 ms to convert the pulse ion signals into analog signals. The signals were further smoothed by passing through a dc amplifier with a 1-kHz band-pass filter before they were introduced into the measuring system described in Section 6.6. The resulted pulse-height spectra for monodisperse aerosols, however, exhibited broad distributions, though the sensitivity was far greater than those in ICP-AES.

The signal intensities and their fluctuations from individual particles were found to be strongly affected by carrier gas flow rate, RF power and sampling depth.[62)] In order to obtain sharp pulse height spectra, the operating conditions were extensively examined with the various combinations of these parameters. Under the optimum conditions finally obtained (carrier gas flow rate of 0.8 l/min, RF power of 1.4 kW and sampling depth of 14 mm), sharp pulse height distributions were resulted. The RSD of the distribution was 5 %, which was even better than the typical RSD of 11 % obtained in ICP-AES.[47)] The detection limit of zinc in a particle was estimated to be 3 fg.

7. 7 Laser Ablation for ICP-MS

The laser ablation technique became one of the popular sampling method for solid samples in ICP-AES and ICP-MS. The application of this method in ICP-AES was described in Section 6.5. The vaporization process of samples by the laser ablation is not so stable, which consequently deteriorates the precision of this method compared to that using the nebulization technique for solution samples. Usually, therefore, the internal standard method is employed by using the matrix or concomitant elements in the sample as an internal standard element.

If the amounts of sample vapor introduced into the plasma can be measured, signal intensities might be corrected. In order to measure the aerosol density of the ablated materials, a laser light scattering cell was constructed similar to the one described in Section 6.6.3 and inserted into the transport tube of the sample vapor from the laser ablation chamber to ICP torch.[63)] The signals from the laser light scattering cell were integrated for 12 s in a single pulse ablation mode. The Nd: YAG laser was operated in free running mode at an energy of 150 mJ.

In the single pulse mode, the RSD of the average ion intensities of Co and Mo for zircalloy samples ranged from 7 to 60 %, while the RSD of the normalized intensities by the scattered light ranged from 4 to 18 %. The improvement of the precision is apparent and this method can potentially be used for the local analysis since the sampling at a very small area of *ca.* 100 μm in diameter is possible by a single laser pulse.

Acknowledgments

The author wishes to express his sincere gratitude to his colleagues and many students studied in his laboratory for their collaboration in the works described in this review. Their

names are given in each of the papers listed in the references. These works were partly supported by Grant-in-Aid Scientific Research from the ministry of Education. The author is also indebted to many companies for their financial support and instrument donation and wishes to express his deep appreciation to them. These companies include Asahi Glass Foundation for Industrial Technology, Mitsui Mining & Smelting Co. Ltd., Kawasaki Steel Co., Nippon Steel Co., NKK Co., Seiko Instruments Inc., and Perkin-Elmer Japan Co., Ltd.

References

1) S. Greenfield, I. L. Jones, C. T. Berry, "High-Pressure Plasmas as Spectroscopic Emission Sources", *Analyst*, **89**, 713 (1964).
2) R. H. Wendt, V. A. Fassel, "Induction-Coupled Plasma Spectrometric Excitation Source", *Anal. Chem.*, **37**, 920 (1965).
3) G. W. Dickinson, V. A. Fassel, "Emission Spectrometric Detection of the Elements at the Nanogram per Milliliter Level Using Induction-Coupled Plasma Excitation", *Anal. Chem.*, **41**, 1021 (1969).
4) R. S. Houk, V. A. Fassel, G. D. Flesch, H. J. Svec, A. L. Gray, C. E. Taylor, "Inductively Coupled Argon Plasma as an Ion Source for Mass Spectrometric Determination of Trace Elements", *Anal. Chem.*, **52**, 2283 (1980).
5) A. L. Gray, A. R. Date, "Inductively Coupled Plasma Source Mass Spectrometry Using Continuum Flow Ion Extraction", *Analyst*, **108**, 1033 (1983).
6) T. Takahashi, S. Murayama ed., "Emission Spectrometry for Liquid Samples, Mainly Using ICP", Gakkai Shuppan Center, Tokyo (1983).
7) H. Haraguchi, "Fundamentals and Application of ICP Emission Spectrometry", Kodansha, Tokyo (1986).
8) P.W.J.M. Boumans, "Inductively Coupled Plasma Emission Spectroscopy, Pt. 1 and 2", John Wiley & Sons, New York (1987).
9) V. A. Fassel, R. N. Kniseley, "Inductively Coupled Plasma-Optical Emission Spectroscopy", *Anal. Chem.*, **46**, 1110A (1974).
10) H. Kawaguchi, "New Spectroscopy and its Application, (5) Optical Emission Spectrometry with an Inductively Coupled Plasma as Light Source", *J. Spectroscop. Soc. Japan*, **27**, 387 (1978).
11) H. Kawaguchi, T. Ito, A. Mizuike, "Determination of Phosphorus in Various Samples by Inductively Coupled Plasma-Optical Emission Spectrometry", *Bunseki Kagaku*, **27**, 53 (1978).
12) H. Kawaguchi, "The Determination of Temperatures of Light Sources for the Spectroscopic Analysis from Spectra", *J. Spectroscop. Soc. Japan*, **13**, 1 (1964).
13) H. Kawaguchi, T. Ito, A. Mizuike, "Axial Profiles of Excitation and Gas Temperatures in an Inductively Coupled Plasma", *Spectrochim. Acta*, **36B**, 615 (1981).
14) H. Kawaguchi, Y. Oshio, A. Mizuike, "Interferometric Measurements of Spectral Line Widths Emitted by an Inductively Coupled Plasma", *Spectrochim. Acta*, **37B**, 809 (1982).
15) H. Kawaguchi, T. Ito, K. Ota, A. Mizuike, "Effects of Matrix on Spatial Profiles of Emission from an Inductively Coupled Plasma", *Spectrochim. Acta*, **35B**, 199 (1980).
16) T. Ito, H. Kawaguchi, A. Mizuike, "Effect of Organic Solvent on the Inductively Coupled Plasma Impedance", *Bunseki Kagaku*, **28**, 648 (1979).
17) J. Xu, H. Kawaguchi, A. Mizuike, "Effects of Organic Acids and Solvents in Inductively-Coupled Plasma Emission Spectrometry", *Anal. Chim. Acta*, **152**, 133 (1983).
18) H. Kawaguchi, M. Okada, T. Ito, A. Mizuike, "Computer-Controlled Programmable Monochromator with Repetitive Optical Scanner for Accurate Peak Detection and Background Correction", *Anal. Chim. Acta*, **95**, 145 (1977).
19) T. Sakamoto, M. Okada, H. Kawaguchi, A. Mizuike, "Gas Chromatography of Traces of Beryllium Using the Microwave Plasma Detector", *Bunseki Kagaku*, **25**, 85 (1976).

20) H. Kawaguchi, T. Ito, M. Okada, A. Mizuike, "On-Off Control Unit Utilizing Digital-to-Analog Converter Output of Minicomputer System", *Bunseki Kagaku*, **26**, 564 (1977).
21) M. Okada, H. Kawaguchi, A. Mizuike, "Signal-to-Noise Improvement in Emission Spectrometry by Repetitive Optical Scanning and Data Processing with a Minicomputer", *J. Spectroscop. Soc. Japan*, **25**, 194 (1976).
22) M. Hiraide, T. Ito, M. Baba, H. Kawaguchi, A. Mizuike, "Multielement Preconcentration of Trace Heavy Metals in Water by Coprecipitation and Flotation with Indium Hydroxide for Inductively Coupled Plasma-Atomic Emission Spectrometry", *Anal. Chem.*, **52**, 804 (1980).
23) H. Kawaguchi, T. Ito, A. Ito, A. Mizuike, "A Method of Data Processing for Improving Precision of Intensity Measurements in Inductively-Coupled Plasma Emission Spectrometry with a Programmable Monochromator", *Anal. Chim. Acta*, **122**, 75 (1980).
24) H. Kawaguchi, "Principle and Application of Echelle Spectrometers", *Bunseki*, No.7, 62 (1984).
25) H. Kawaguchi, K. Yoshimura, A. Mizuike, "Some Characteristics of a Commercial Echelle Spectrometer", *Spectrochim. Acta*, **41B**, 295 (1986).
26) J. Xu, H. Kawaguchi, A. Mizuike, "Spectral Interferences in the Determination of Phosphorus in Steel by Inductively Coupled Plasma Emission Spectrometry with an Echelle Monochromator", *Appl. Spectrosc.*, **37**, 123 (1983).
27) H. Kawaguchi, K. Ota, T. Ito, A. Mizuike, "A Multichannel Spectrometric System with a Photodiode Array Detector", *J. Spectroscop. Soc. Japan*, **29**, 115 (1980).
28) H. Kawaguchi, "Data Processing for Image Detector. A Spectrometric System with a Photodiode Array Detector", *Kagaku no Ryoiki*, **36**, 799 (1982).
29) H. Kawaguchi, K. Hattori, T. Ito, A. Mizuike, "Characteristics of an Image Dissector as a Detector for Emission Spectrometry", *J. Spectroscop. Soc. Japan*, **33**, 179 (1984).
30) H. Kawaguchi, Y. Hotta, A. Mizuike, "ICP-AES with an Image Dissector Tube as Detector", *Bunseki Kagaku*, **36**, 453 (1987).
31) H. Kawaguchi, T. Ito, S. Rubi, A. Mizuike, "Water-Cooled Torch for Inductively Coupled Plasma Emission Spectrometry", *Anal. Chem.*, **52**, 2440 (1980).
32) H. Kawaguchi, T. Tanaka, S. Miura, J. Xu, A. Mizuike, "Analytical Performance of the Water-Cooled Torch for the Inductively Coupled Plasma", *Spectrochim. Acta*, **38B**, 1319 (1983).
33) H. Kawaguchi, T. Tanaka, A. Mizuike, "Analytical Performance of the Axially Viewed Inductively Coupled plasma Generated with a Water-Cooled Torch", *Bunseki Kagaku*, **33**, 129 (1984).
34) C. Li, T. Tanaka, H. Kawaguchi, "A Spray Chamber with Smaller Memory Effect for ICP-AES", *Bunseki Kagaku*, **39**, 367 (1990).
35) T. Ito, H. Kawaguchi, A. Mizuike, "Inductively Coupled Plasma Emission Spectrometry of Microliter Samples by a Flow Injection Technique", *Bunseki Kagaku*, **29**, 332 (1980).
36) T. Ito, E. Nakagawa, H. Kawaguchi, A. Mizuike, "Semi-Automatic Microliter Sample Injection into an Inductively Coupled Plasma for Simultaneous Multielement Analysis", *Mikrochim. Acta*, I, 423 (1982).
37) S. Rubi, T. Ito, H. Kawaguchi, A. Mizuike, "Determination of Trace Rare Earths in Carbon Steel by Microliter Sample Injection-ICP Emission Spectrometry", *J. Chem. Soc. Japan*, No.1, 172 (1981).
38) H. Kawaguchi, M. Hasegawa, A. Mizuike, "An Ultrasonic Aerosol Generator of Emission Spectrometry", *Bunseki Kagaku*, **20**, 893 (1971).
39) H. Kawaguchi, T. Saga, A. Mizuike, "Emission Spectrographic Analysis of Solutions by DC-Arc Excitation with an Ultrasonic Nebulizer", *J. Spectroscop. Soc. Japan*, **24**, 99 (1975).
40) H. Kawaguchi, T. Tanaka, A. Mizuike, "An Ultrasonic Nebulizer for Microliter Samples in Inductively Coupled Plasma Emission spectrometry", *Bull. Chem. Soc. Japan.*, **55**, 3033 (1982).
41) H. Kawaguchi, B.L. Vallee, "Microwave Excitation Emission Spectrometry. Determination of Picogram Quantities of Metals in Metalloenzymes", *Anal. Chem.*, **47**, 1029 (1975).
42) T. Sakamoto, H. Kawaguchi, A. Mizuike, "Introduction of Samples into a Microwave-Induced Argon Plasma Using a Tungsten Filament and a High-Capacity Condenser", *J. Spectroscop. Soc. Japan*, **25**, 35 (1976).

43) H. Kawaguchi, G. Zhan, A. Mizuike, "Electrothermal Vaporization for Sample Introduction into ICP", *Bunseki Kagaku*, **35**, 972 (1986).
44) H. Kawaguchi, J. Xu, T. Tanaka, "Inductively Coupled Plasma-Emission Spectrometry Using Direct Vaporization of Metal Samples with a Low-Energy Laser", *Bunseki Kagaku*, **31**, E185 (1982).
45) H. Kawaguchi, N. Fukasawa, A. Mizuike, "Investigation of Airborne Particles by Inductively Coupled Plasma Emission Spectrometry Calibrated with Monodisperse Aerosols", *Spectrochim. Acta*, **41B**, 1277 (1986).
46) H. Kawaguchi, K. Kamakura, E. Maeda, A. Mizuike, "Direct Aerosol Introduction/ICP-AES; Relation between the Decreasing Rate of Particle Number Density and Particle Size", *Bunseki Kagaku*, **36**, 431 (1987).
47) T. Nomizu, H. Nakashima, Y. Hotta, T. Tanaka, H. Kawaguchi, "Simultaneous Measurement of the Elemental Content and Size of Airborne Particles by Inductively Coupled Plasma Emission Spectrometry Combined with the Laser Light-Scattering Method", *Anal. Sci.*, **8**, 527 (1992).
48) T. Nomizu, S. Kaneco, T. Tanaka, D. Ito, H. Kawaguchi, B.L. Vallee, "Determination of Calcium Content in Individual Biological Cells by Inductively Coupled Plasma Atomic Emission Spectrometry", *Anal. Chem.*, **66**, 3000 (1994).
49) H. Kawaguchi, "Inductively Coupled Plasma Mass Spectrometry", *Anal. Sci.*, **4**, 339 (1988).
50) H. Kawaguchi, T. Nakahara ed., "Plasma Ion Source Mass Spectrometry", Gakkai Shuppan Center, Tokyo, (1994).
51) H. Kawaguchi, T. Tanaka, T. Nakamura, A. Mizuike, "Construction of ICP/Mass Spectrometer and its Characteristics", *Bunseki Kagaku*, **36**, 271 (1986).
52) H. Kawaguchi, K. Asada, A. Mizuike, "Optical Characteristics of an Afterglow Extracted from an Inductively Coupled Plasma", *Mikrochim. Acta* [Wien], III, 143 (1988).
53) H. Kawaguchi, T. Tanaka, A. Mizuike, "Continuum Background in Inductively Coupled Plasma Mass Spectrometry", *Spectrochim. Acta*, **43B**, 955 (1988).
54) H. Kawaguchi, T. Tanaka, T. Nakamura, M. Morishita, A. Mizuike, "Matrix Effects in Inductively Coupled Plasma Mass Spectrometry", *Anal. Sci.*, **3**, 305 (1987).
55) Y. Kim, H. Kawaguchi, T. Tanaka, A. Mizuike, "Non-spectroscopic Matrix Interferences in Inductively Coupled Plasma Mass Spectrometry", *Spectrochim. Acta*, **45B**, 333 (1990).
56) T. Tanaka, K. Yonemura, K. Obara, H. Kawaguchi, "Inductively Coupled Plasma Mass Spectrometry with Low-Power Nitrogen and Oxygen Plasmas", *Anal. Sci.*, **9**, 765 (1993).
57) X. Yan, T. Tanaka, H. Kawaguchi, "Reduced Pressure Inductively Coupled Plasma Mass Spectrometry for Nonmetallic Elements", *Appl. Spectrosc.*, **50**, 182 (1996).
58) T. Tanaka, Y. Sakai, H. Kawaguchi, "Effect of Orifice Diameter of Torch Injector Tube in Inductively Coupled Plasma Mass Spectrometry", *Anal. Sci.*, **11**, 673 (1995).
59) H. Kawaguchi, T. Tanaka, M. Tanabe, A. Mizuike, "Application of a Water-Cooled Torch to Inductively Coupled Plasma Mass Spectrometry", *Anal. Sci.*, **5**, 435 (1989).
60) T. Tanaka, K. Yonemura, M. Tanabe, H. Kawaguchi, "Electrostatically Shielded Water-Cooled Torch for Inductively Coupled Plasma Mass Spectrometry", *Anal. Sci.*, **7**, 537 (1991).
61) T. Nomizu, S. Kaneco, T. Tanaka, T. Yamamoto, H. Kawaguchi, "Determination of Femto-gram Amounts of Zinc and Lead in Individual Airborne Particles by Inductively Coupled Plasma Mass Spectrometry with Direct Air-Sample Introduction", *Anal. Sci.*, **9**, 843 (1993).
62) S. Kaneco, T. Nomizu, T. Tanaka, N. Mizutani, H. Kawaguchi, "Optimization of Operating Conditions in Individual Airborne Particle Analysis by Inductively Coupled Plasma Mass Spectrometry", *Anal. Sci.*, **11**, 835 (1995).
63) T. Tanaka, K. Yamamoto, T. Nomizu, H. Kawaguchi, "Laser Ablation/Inductively Coupled Plasma Mass Spectrometry with Aerosol Density Normalization", *Anal. Sci.*, **11**, 967 (1995).